FACULTY OF INFORMATION TECHNOLOGY AND ELECTRICAL ENGINEERING

Brian Johannes Irvine

AUTOMATED GAIT SEGMENTATION AND TRACKING USING INERTIAL MEASUREMENT UNITS

Master's Thesis
Degree Programme in Biomedical Engineering
December 2020

Irvine B.J. (2020) Automated Gait Segmentation and Tracking Using Inertial Measurement Units. University of Oulu, Degree Programme in Biomedical Engineering. Master's Thesis, 61 p.

ABSTRACT

In this thesis, a methodology is presented to automate the labelling, event detection, segmentation, tracking, and parameter extraction of IMU gait data for sensors placed on the feet and shanks. The algorithms presented were tested using IMU data from three different styles of gait, normal gait, antalgic gait, and limited mobility gait. The algorithms developed were found effective for all of the simulated gait styles without mislabelling or detecting erroneous gait segments. The resultant gait trajectories and parameters were analyzed and were found to accurately depict the differences between each of the different styles of gait.

The methodology presented can be used for the rapid and accurate processing of gait data for multiple styles of gait. This quantification of gait data can enable the collection of IMU gait data on a larger scale. This provides an accessible, low-cost option for out-of-laboratory gait data collection.

Keywords: IMU, Gait Analysis, Gait Temporal Parameters, Gait Trajectories

TABLE OF CONTENTS

FOREWORD

This thesis is the culmination of my studies at the University of Oulu. I consider it the keystone of my learning here and it would not have been possible without the foundation laid by my other courses and life experiences. As a lifelong learner I expect to further build on this experience. I am truly grateful to have been able to perform this work in such a rewarding field.

This work would not have been possible without the everlasting support, patience, and understanding of my friends and family. Finally, I would like to thank Tapio Seppänen and Kai Noponen for their patience and support throughout the entire project.

Oulu, 03.12.2020

Brian Johannes Irvine

ABBREVIATIONS AND SYMBOLS

AHRS	attitude and heading reference system
DOF	degrees of freedom
EC	end contact
EFC	end full contact
EMG	electromyography
GE	gait events
GTP	gait temporal parameters
IC	initial contact
IFC	initial full contact
IMU	inertial measurement unit
MARG	magnetic, angular rate, and gravity sensor
MEMS	micro electromechanical system
PD	Parkinson's disease

EC_k	time of k^{th} occurrence of EC event
IC_k	time of k^{th} occurrence of IC event

Σ	frame of reference
R	frame rotation matrix
a	linear acceleration
$\bar{a}$	linear acceleration with gravity removed
t	time
t_0	initial time
α	roll angle
γ	yaw angle
θ_P	pronation angle
θ_I	in-turn angle

$[\ ]^T$	transpose

1. INTRODUCTION

Walking is an essential activity of daily living for many people. Often oversimplified, walking is a complex activity made possible by the cooperation of different body systems to sense the orientation of the body and provide feedback which leads to motion. The result is the ability to provide locomotion while maintaining balance.

Not everyone has the same style of walking. It is impacted by the performance of each system which makes walking possible. Walking abnormalities can be a result of impairment to the musculoskeletal or nervous systems. Perhaps the most simple explanation of gait analysis is that "gait analysis is the process of determining what is causing patients to walk the way they do." [1].

Clinical gait analysis is used for a variety of reasons, to assess an individual's need for orthopaedic surgery, to develop compensatory strategies in rehabilitation, or recently even to discern between neurological disorders. In all of these cases the quality of data is paramount in order to provide the proper surgery, rehabilitation, or diagnosis. Because, of this requirement of high-quality data, much of the clinical gait analysis is done using motion capture, force plates, or the professional observation of high-speed video. These methods contribute to a high cost of analysis and enforce an additional constraint that gait analysis must be performed within a clinic or laboratory.

The increasing performance of inertial measurement units (IMU) is making them a viable tool for clinical gait analysis. The IMU benefits from its relatively low cost compared to other modalities. Compared to motion capture the IMU has a lower setup time, because fewer sensors are required than the number of markers for viable motion capture. The IMU also benefits from a much wider collection environment which expands beyond the walls of the laboratory. With a wireless IMU module, like the one described in this thesis, collection can be done in the laboratory, at home, outside, or anywhere that has a flat and safe surface to walk on. This allows for the collection of data from many more strides than is possible with motion capture, force plate, or professional observation.

Compared to professional observation, the IMU measurements have the additional benefit of being quantitative. This removes observational bias and allows for the calculation of non-discriminatory gait parameters. These gait parameters can them be studied by gait pathologists to determine the source of the gait abnormality and suggest treatment in the form of surgery or rehabilitation. The added benefit of these quantitative measures is that they allow for gait analysis to be done by machine learning models which will be exhibited in the literature review to have a significant ability to distinguish between neurological gait pathologies.

This thesis proposes a tool to help with the quantification of IMU gait data. The tool is a data pipeline which was developed to automatically label sensors, detect gait events, remove gait artefacts, and produce organized and meaningful gait parameters. This thesis will follow this process of developing this pipeline from the sensor level to the extraction of gait parameters. This pipeline will prove useful in the rapid processing of large amounts of gait data produced by the IMU as collection becomes more ubiquitous. With the low cost of collection and the ability to collect data outside of the laboratory. This means that gait data measured by IMU has the potential to collect vast amounts of walking data by having the patient wear the system as they simply go about their day. As collection becomes more ubiquitous and data volumes increase, the proposed pipeline, or similar data processing strategies will be essential to achieving high-accuracy, low-cost gait analysis.

2. LITERATURE REVIEW

Walking is a critical activity of daily living for many people. Being able to walk efficiently is a certain improvement to quality of life. Not only can walking inefficiently or slowly decrease someone's ability to get around, it can also induce stigma, or lead to injury. Falls that occur during walking due to impairment of gait pose a serious risk to the elderly [2]. The fear of falling and associated reduction in mobility and independence is also a significant detriment to quality of life [3].

It was once believed that gait disorders were an inevitable development associated with aging, however it is now apparent that gait disorders are indicative of specific underlying disorders which warrant diagnostic tests [3]. These underlying condition s include subtle white-matter lesions, vestibular dysfunction, or oculomotor changes [3]. Further testing has the potential to identify the cause of gait abnormalities using a systems-based approach. In some cases the manifestation of gait disturbances, even in isolation, can be a pre-clinical indicator of underlying cerebrovascular or neurodegenerative disease [3]. Gait parameters such as gait speed are also an effective marker of clinical health and is are effective predictors of mortality in older adults [4].

The impact of gait disturbances on quality of life and the potential for gait to be used as a tool for identifying pre-clinical conditions provides apt motivation for the development of new tools and methods for the monitoring of gait. This chapter will discuss current developments in the monitoring of gait and the applications made possible through the quantification of gait. This begins with a more detailed investigation of gait from a systems-based perspective, analyzing the anatomy and physiology which, when unimpeded, enable normal gait.

2.1. Anatomy and Physiology of Gait

Human walking is complicated. It is a result of symphonic cooperation between the nervous system, vestibular system, and musculoskeletal system. The interconnected physiology of systems related to gait is evident in a study by Sejdić in which challenging conditions for gait manifest changes in electrodermal, respiratory, and cardiological function [5]. This provides evidence for considering gait, and by extension, gait abnormalities as an indicator of multi-factor systemic function.

The most common causes of abnormal gait are non-neurological, including those caused by joint pain or a lack of joint mobility [3]. These are effectively a challenge to the musculoskeletal system which preforms gait.

Further impairments to gait can be caused by the nervous system which initiated, controls, and adapts to changes in gait. In the nervous system, gait is "governed by the hierarchical control of the primary motor cortex, premotor and supplemental motor cortices, basal ganglia, cerebellum, brainstem, spinal pattern generators and feedback from the vestibular system." [3] The key functions of neuronal systems during gait are locomotion, balance, and ability to adapt to the environment which are supported by executive, cognitive, and affective dimensions of control [3]. Disruption of the underlying motor or neural system results in inability to complete these functions which manifests as abnormal gait.

The process of walking is highly dependent on cognitive executive function. This has been shown in experiments in which participants are cognitively challenged by additional tasks while walking. The additional cognitive load leads to gait decrements

in healthy and patient populations [3]. This additional cognitive load could reveal underlying gait abnormalities if given the opportunity. In a paper assessing the interaction between physical systems while walking outside, the author suggests that laboratory walking may not provide enough to stress physiological systems [5]. This suggests that testing for specifically neural gait abnormalities should be tested in a way that provides a default cognitive load such as outside environments.

Due to the heavy involvement of the neural function in gait it is no surprise that neurological diseases heavily impact gait. The complexity of the neural systems being affected also means that the manifestations of disease in gait patterns may have disease specific patterns. This has allowed researchers to develop machine learning models which predict neurological disorders based on gait data. An example of this is a study by Mannini et al. which used IMU data and a support vector machine (SVM) classifier to accurately label gait data from healthy individuals, post-stroke patients, and individuals with Huntington's disease [6]. Although successful classifiers like the one mentioned above have been developed and are in constant development, widely applicable algorithms remain very complex because gait disorders are a result of concurrent effects from multiple causal factors [7].

Gait analysis involves measuring the spatial and temporal aspects of walking [1]. Spatial measurements include step length and step width [1]. One step is defined as the movement of one foot to be in front of the other while a stride, consisting of two steps, begins and ends with the same foot returning to its initial position [1]. Temporal aspects of gait are the times required for different motions in walking and include step times or times spent in different phases of gait [1]. Spatial and temporal parameters of interest in this work will be discussed further in sections 2.7 and 2.8.

2.2. Methods for Collection of Gait Data

Gait abnormalities are commonly evaluated through combination of observation, functional assessment and questionnaires [8]. However, this can be problematic due to observational bias and lack inter-rater reliability [8]. This was somewhat alleviated by the introduction of video capture systems which allow for observation by multiple professionals to develop a second opinion. However, largely these issues remained and have motivated a change in the way that gait is studied from qualitative to quantitative analysis.

The first widespread use of quantitative gait analysis used electromyography (EMG) to measure muscle activity [1]. EMG measures the electrical activity produced by the activation of motor units [1]. Electrodes could be placed over any superficial muscles in the thigh or shank to monitor muscle activity. This could be used to determine asymmetry between legs or to diagnose medical conditions. However, now the use of EMG is no longer the norm for clinical gait analysis [1].

Kinematic monitoring of gait using motion capture and force plates has become the norm for clinical gait analysis. Technological advancement in the field led to the development of 3D motion capture and force plate systems [8]. Motion capture works by placing markers on the subject which are detected by a series of cameras surrounding the capture area. Markers are detected by the cameras simultaneously and the 3D location of each marker is reconstructed through comparison of camera images [1]. This gold standard in gait analysis provides high quality data, but is expensive to acquire and maintain and has a very limited range within the constrained environment of a laboratory [8]. Additionally, these systems require qualified personnel to operate

and interpret their results [9]. This high cost makes motion capture systems a luxury, motivating other technologies to provide lower cost, more widely applicable solutions.

There are also lower cost vision based systems such as the Reha@home mentioned in a comparison of vision-based and sensor based systems for join angle gait analysis by Kyrarini, Wang, and Graser [10]. However, these systems still have the consequence of being location dependent and can only work within a constrained capture area. These systems have also faced issues with the assessment of gait parameters. A low-cost vision-based system using Microsoft Kinect™ was compared to a Vicon 3D motion capture in a study by Pfister et al. [11]. It was found that the Kinect™ based system inaccurately reported joint angles and was declared by the authors as not suitable for clinical use [11].

Other solutions focus on using sensors like inertial measurement units (IMU) to collect data outside of the laboratory. Of all of the sensors used in out-of-laboratory gait analysis, IMU seem to be the most popular, because they are lightweight, low-cost sensors which produce high quality acceleration and angular position data at high sampling rates. A study by Sabatini et al. was the first to show how accelerometer data could be used to create accurate measurements of foot position during gait [12]. IMU is sometimes supplemented with other technologies as in the case of the Xsens ForceShoe™ which combines two IMU with two 3D force and motion sensors to produce an ambulatory gait lab which has been validated against the gold standard of 3D motion capture [13].

Often the best results in gait analysis have come from multimodal approaches. An example of this is a system developed by Rodrigues et al. which improved the accuracy of a marker-less vision based system using the Microsoft Kinect™ which achieved 95% accuracy compared to Vicon 3D by adding IMU sensors on the shank and thigh [9].

2.3. Inertial Measurement Unit (IMU)

The IMU is a relatively complex sensor made up of multiple components. By definition an IMU contains at least an accelerometer and a gyroscope with the magnetometer considered as optional. In this thesis, the magnetometer will always be included in the definition of an IMU. IMU are available with different numbers of degrees of freedom (DOF). In this thesis, the IMU will be considered to have 9 DOF, 3DOF for each orthogonal direction of the accelerometer, gyroscope, and magnetometer. Some IMU like the one used in this study, contain a temperature sensor for compensation of sensor drift due to temperature change. IMU vary in many aspects including price, size, accuracy, and amount of onboard processing.

The IMU used for this project are microelectronic mechanical system (MEMS) IMU. MEMS IMU are desirable for their small form factor and weight. MEMS IMU use miniature mechanical systems which deform when an acceleration, angular velocity, or magnetic field is applied. The deformations in the miniaturized mechanical system produce electrical signals which are converted to digital signals by and onboard processing unit. The mechanism for each of the IMU components will be described in greater detail in the following sections. MEMS sensors are not as accurate as their tactical grade equivalents, but they have advantages in terms of smaller size, lower power, and lower cost of implementation [14]. MEMS IMU sensors suffer from bias, noise, scaling errors, non-linearity, temperature effects, and misalignment errors [14].

For these reasons it is important to have software solutions to extract meaningful data. It is possible to implement software solutions to these issues and many distributors of MEMS IMU include this software with the devices. Figure 1 shows an image of the Hillcrest FSM-9, a 9 DOF IMU, which was used in this thesis.

Figure 1. Hillcrest FSM-9 9-axis inertial measurement unit (IMU) (CEVA, 2019).

The accelerometer is responsible for measuring the acceleration of the sensor including the acceleration effects produced by gravity. These acceleration signals are produced by the motion of a proof mass through a substrate with a fixed electrode on either side[15]. The motion of the proof mass changes the capacitance between the plates which is then measured as a proxy for acceleration [15]. One accelerometer is required for each DOF of the accelerometer.

The vector of acceleration due to gravity is known to be $9.81 m/s^2$ straight up, orthogonal to the surface of the Earth. This is important for determining the orientation of the sensor. The acceleration can also be integrated to get velocity and twice to get position. However, integration introduces a lot of drift error through the summation of sensor noise. For this reason, getting an accurate sensor is essential when the integrals of acceleration are desired.

Angular velocity is measured by an onboard gyroscope. The MEMS gyroscopes can use a variety of techniques to measure vibrations imposed by the Coriolis effect when the sensor is rotated [16]. This is commonly measured using a tuning fork whose tines oscillate upon rotation. The Coriolis force can then be measured based on the differential bending of the tines or by the vibration of the stem [16]. Again, one of these units is required for each DOF of the sensor.

The magnetic field is measured with an onboard magnetometer which functions through a variety of methods for measuring the resistance of two piezo resistors attached to a U-shaped cantilever beam. When introduced to a magnetic field the cantilever beam induces strain in the two sensors which is converted to an electrical signal via Wheatstone bridge [17]. Knowledge of the Earth's ambient magnetic field is useful because it is static and can therefore be used in conjunction with the vector of acceleration due to gravity in order to determine orientation.

2.4. Gait Events (GE) and Gait Temporal Parameters (GTP)

Gait is a cyclic process punctuated by gait events. The gait cycle begins with a specific gait event of one foot with the ground and lasts until the same gait event repeats itself [18]. The gait cycle can be broken down with varying degrees of granularity which are summarized in a well-received article by Taborri et al. [18]. These levels of granularity include 2-8 phase models of gait, with increasing specificity with each additional phase. The simplest of these is the two-phase gait model which only shows stance

phase, when the foot is in contact with the ground, and swing phase, when the foot is not in contact with the ground. Taborri et al. notes that the two-phase gait model is sufficient for most applications of functional electrical stimulation (FES) and for the actuation of assistive motors in exoskeletons [18]. This is a meaningful statement, because it shows that complexity is not always required and increasing the number of phases is unnecessary in some cases and can be costly. This is because increasing the number of phases also increases the demands on hardware and software, without returns in real-world applicability. Increasing granularity allows for a greater ability to differentiate between gait activities or assess pathological gait [18]. This thesis will focus on the four-phase gait model which consists of the loading response, flat foot, pre-swing, and swing phases which begin with initial contact (IC), initial full contact (IFC), end full contact (EFC), and end contact (EC) respectively. It should be noted that naming of gait events and phases is not always consistent.

Gait temporal parameters are the standard quantifications of gait, perhaps because they can be uniformly and accurately measured using so many different modalities, from foot switches to IMU [19]. Gait events are detected using a variety of algorithms including foot switches, foot pressure insoles, linear accelerometers, gyroscopes, IMU, EMG, electroneurography, ultrasound, force platforms, and opto-electronic systems [18]. When using IMU, gait events are generally based on the target variables of acceleration and/or angular velocity [20]. For this thesis, gait events will be detected based on angular velocity which was used by Jasiewicz et al. [19]. This algorithm will be explained in detail in section 5.4.

2.5. Gait Orientation and Position Trajectories

Orientation and position tracking are important measurements because they provide data which is easily understood. They also provide essential spatial data which can be used in the detection and understanding of abnormal gait. However, this is problematic when measuring walking using IMU orientation and position are not default outputs, they require calculation based on the accelerometer, angular velocity, and magnetometer signals.

Orientation estimates are produced by time-integrating with known initial conditions [21]. These estimations are sensitive to gyroscope drift but can be helped by the known acceleration due to gravity and the assumption of a homogenous magnetic field [21]. The Earth's ambient magnetic field vector can be used in conjunction with the ambient gravity vector to determine orientation by providing two known vectors with which to orient the sensor [22]. Seel, Raisch, and Schauer cite potential issues with this reasoning as the orientation of the sensor and actual body segment may not align, and that in practice the magnetic field is prone to ferromagnetic distortion [23]. For this reason, in a subsequent paper, Seel, Graurock, and Schauer decided to leave out the magnetometer entirely when developing their algorithm for orientation estimation [24]. This required an assumption of unchanging orientation between flat foot segments [24]. From accurate, globally referenced, orientation it is also possible to produce joint angle measurements which open up more possibilities for gait analysis.

Another challenge with using the IMU for gait analysis is in measuring linear velocity (ie. walking speed), or position. The challenge is that one cannot simply integrate the acceleration measurements to calculate these values. This is partially due to the effect of gravity which results in a constant acceleration on the sensor, with no

associated motion [25]. Another issue is that drift errors in the accelerometer accumulate very quickly when integrated [25]. Sabatini et al. proposed a partial solution to this by resetting the integration for each stride [12]. This was enabled by setting initial conditions for the integration based on the moment when the foot is flat and the shank is vertical and there is not linear or angular acceleration of the foot [12]. A similar technique was used by Kitagawa and Ogihara to achieve step-by-step foot trajectories which estimated stride length with an average error of only 20±50mm and foot clearance with an average error of 2±7mm [26]. A very impressive result compared to the 1mm error assumed with the gold standard VICON 3D motion capture [26].

Another, rather unique solution to the problem of position tracking by IMUs was implemented by Roetenburg et al. By creating an augmented magnetic field using wearable magnetic coils [27]. This allows low-frequency magnetometer based observations of position to correct for integration drift through the use of a Kalman filter [27]. This is effectively the same as the other algorithms which use the Earth's magnetic field, but with a much high signal-to-noise ratio (SNR) and much lower influence from external ferromagnetic disturbances.

2.6. Assessment of IMU Gait Data Quality

Error in IMU-based gait measurement can be studied in several different ways. The most popular is to compare the gait temporal parameters calculated with the IMU to a gold standard measurement system, such as motion capture [27], [28], force plate [8], [20], or stereophotogrammetry. This is a measure of validity. Washabaugh et al. measures the validity of IMU based measurement of gait temporal parameters by comparing the IMU GTPs to those would by a force plate [8]. The authors of this study also measure repeatability of IMU systems by having participants monitored on consecutive days, assuming that they will have the same gait parameters [8]. The result of this study was that the IMU gait measurement system had both a high validity and repeatability for healthy young adults [8].

Another way of calculating the error is through absolute error testing. This requires the IMU to be moved in such a may that the ground truth motion parameters are known. This is not very common but has been performed by Ricci, Taffoni, and Formica. In this study, IMUs were rigidly fixed to a robotic arm and moved at frequencies indicative of human gait [29]. They authors tested different sensor fusion methods for dynamic and static measurements [29]. Absolute measurements like this are highly desirable, but very difficult to achieve, for this reason relative error measurement methods are generally used instead. Ricci, Taffoni, and Formica used relative error measurements defined as the piecewise difference between two sensors in their measurement of the same orientation [29]. They define the orientation difference as the length of the shortest path between two quaternions [29].

2.7. Gait Data in Rehabilitation and Assistive Devices

Another topic in gait analysis is rehabilitation. Rehabilitation is often the combination of gait quantifications with therapy, often occurring in a cycle to meet patient needs over time. This repetition means that the data needs to be repeatable and have a low minimum discernable change (MDC) so that improvement of gait parameters can

attributed to therapy rather than error [8]. In these cases, it would also be beneficial to have a greater number of steps measured and in a greater number of environments. This provides motivation for portable systems for gait analysis. This motivates the use of IMU to preform measurements because they do not rely of a laboratory environment and can take place in uncontrolled environments where the participant will have minimal impacts to the naturality of their gait.

In addition to monitoring gait to come up with therapeutic solutions it is also possible to use the online processing of gait data to build assistive robotic devices such as the exoskeleton built by Bae et al. [30]. This soft and light exoskeleton uses IMU sensors attached laterally to the foot to detect gait events [30] . The system controller used the gait events to provide assistance at the correct time to compensate for weakened or asymmetric gait in post-stroke patients [30]. This is one example of how online gait collection and processing can enable people to improve their gait, and the associated quality of life. This also highlights the necessity of accurate measurements. If gait events were detected at the wrong times, then the actuations would occur at the wrong time and gait could be further impaired.

Although this thesis focuses primarily on offline methods of gait analysis, there are shared features such as the collection of good data for processing by using a sound methodology and effective sensor placements. Offline data could also provide as training information for future machine learning algorithms to run online.

2.8. Gait Data in Diagnosis

Gait is commonly used to diagnose and evaluate the severity of neurological disorders that modify the movement of the body. The most common disease in this category is Parkinson's disease (PD) [31]. The primary symptoms of PD are the lack of postural stability, tremors, and movements that can be slow or halting [31]. Given that these effects all manifest in gait it makes sense that it would be possible to diagnose and estimate the progression of the disease. Even with many features appearing in gait, it is difficult to design machine learning models appropriate to differentiating these subtleties from the subtleties of normal gait [32]. Cuzzolin et al. proposed an algorithm to deal with this by encoding gait parameters within hidden Markov models to represent gait data over a fixed-length [32]. The algorithm then uses a nearest neighbor classifier to classify the gait as indicative of Parkinson's disease or normal gait [32]. The algorithm was considered successful, with an accuracy of 85.51% and a sample size of 156 people [32]. The ability of IMU data to potentially diagnose neurological conditions also includes post-stroke patients [6], patients with Huntington's disease [6], and patients with multiple sclerosis[33] .

In the diagnosis of neurological disorders such as Parkinson's disease (PD) , it is the momentary status of the patient that is being analyzed [31]. This motivates repeated measurements to measure progression of symptoms. One of the benefits of using gait analysis for tracking neurological disorders is that with the right equipment, the IMU, repeat measurements can be repeated regularly at low cost. This provides a more holistic understanding of disease progression and could improve the quality of care and treatment received by individuals with neurological conditions.

3. HARDWARE AND DESIGN

The first step of gait analysis is converting the real-world event of gait into electrical signals which can be processed. If accurate gait data is desired, it is essential to ensure that the system inputs of acceleration, angular velocity, and magnetic field from the IMU are as accurate as possible. Even the best algorithms for gait analysis will be useless if the input data is inadequate. This chapter follows the process of designing a system to collect, synchronize, and save data from IMU for the purpose of offline processing of gait data.

3.1. IMU Sensor Selection

As mentioned above, sensor accuracy is paramount to a successful gait analysis system. However, accuracy is not the only criterion of importance, size, weight, interactivity, technical support, and sampling rate are additional factors which needed to be considered. High accuracy is important in ensuring high-quality data. Small size and weight are important in ensuring the subjects ability to perform natural gait. IMU sensors with options for simple interactivity through USB interfaces are preferential for this development case, because they enable rapid prototype development and simple interchangeability of components. Actionable technical support in the form of open-source libraries is important, because it greatly reduces development time. Finally, sampling rate should be high in order to not miss out on potential high-frequency signals.

The selected sensor, the FSM-9 by Hillcrest Labs was chosen for its marriage of small size and weight with high accuracy and a relatively high data rate. The FSM-9 collects accelerometer, gyroscope, and magnetometer at 500Hz and can produce sensor fusion outputs at 250Hz. The FSM-9 is also factory calibrated [34].The accuracy of the FSM-9 is also quite good, based on the Hillcrest FSM-9 reference material which is cited in part in table 1 [34]. This table also shows that sensor has sufficient resolution to provide a smooth signal. Additionally, the sensors have relatively little bias, due to the factory calibration. Finally, the range of the FSM-9 includes the ranges of acceleration (±4g) and angular velocity (±500˚/s) characteristic of human gait [12]. Having sufficient range ensures that there is no sensor clipping.

Table 1: Summary of sensor specifications for the FSM-9 taken directly without unit conversion from the Hillcrest FSM-9 Data Sheet [34]

	Linear Acceleration	Angular Velocity	Magnetometer
Range	±8g	±1833˚/s	±600μT
Resolution	< 6mg	0.04˚/s	< 1μT
Bias	< 20mg	0.01rad/s	< 5μT
Non-Linearity (% full scale)	0.5%	0.2%	0.5%

In addition to these impressive specifications the FSM-9 has also built a reputation through use in other peer reviewed articles [10], [35]. In one of these studies the FSM-

9 was show to be able to measure joint angles within 3 degrees of error compared to a PASCO PS-2138 goniometer ground truth [10]. Its use in existing academic literature suggests that the sensor is of sufficient quality for modern academic research.

The FSM-9 also had some quality-of-life improvements in terms of development over other sensors. One of these is that each sensor is factory calibrated using a highly controlled gimbal. The sensor outputs are also subjected to dynamic calibration over changing time and temperature [34]. The FSM-9 also uses a predefined communication protocol with open source libraries for programming data collection [36]. The inclusion of a USB interface for simplified data transmission compared to I2C or SPI. USB provides a better interface for this application, because it allows easy assembly, disassembly, and replacement of components. It also reduces modes of failure introduced by soldered joints on the sensors.

3.2. Sensor Controller Selection,

A sensor controller was designed to receive and save the streamed data from the IMU sensors. The Raspberry Pi 4 B computer was selected as the processing unit for the data collection device. It was selected for its small size, ability to run for hours powered by a relatively small battery, abundance of USB ports for connection to the IMU sensors, and its native Wi-Fi support which allows it to run an Apache Server and be accessed remotely. Finally, the controller needed to have accurate time signals provided by a real time clock (RTC). The RTC used for this project was the ChronoPi 1.0. The Raspberry Pi was supported in an adjustable waist pouch with its accompanying battery pack.

3.3. Device Programming, Communication, and Networking

Collection of data from the sensors was simplified by the inclusion of the publicly available Hillcrest Freespace libraries (Hillcrest Labs, Mountain View, USA). Communication protocols are included in the HCOMM Reference Manual [36]. However, changes and additions needed to be made to the code base to only collect the required data. The code was also edited to provide multi-device scaling and synchronization. Interfacing with the IMU occurs through the sending of data requests and the subsequent receiving of the requested data. A system of asynchronous collection was selected, because it allowed for collection at higher sampling rates than synchronous collection which would face major delays at higher sampling rates. In this way the sensors are initialized, set to the proper sampling rate by a motion data request, then set to stream data continuous until reset or turned off. Importantly each sensor sends the motion data packet with fields indicating the numerical sensor ID and sequence number. The sequence number is a monotonically increasing integer applied to each packet which allows for the detection of any packets lost in transmission. The device ID and sequence number combined with the time stamp applied to the packet on arrival by the Raspberry Pi allow for the real-time determination of sampling rate for each sensor. The desired features from each packet are extracted and written to a csv file. This process is contained in two executable programs, one for initialization and setting the data rate and the other for collecting gait data.

The two executable files were then made executable over a network connection. By running an Apache server with PHP on the Raspberry Pi it is possible to create a

series of web pages have access to run these executables on the Raspberry Pi. In this way, the person collecting the data could log on to the local area network on a computer or a smartphone and be able to set the device data rate, collect data, and reboot the Raspberry Pi if necessary. In the future this network could be expanded by connecting the Raspberry Pi to the internet and enabling remote access. However, this would require security improvements as the current device, and the data on it, is primarily controlled by limiting access to the network. In order to restrict unauthorized access to the server, the controller and the network and communications were encrypted using standard wifi methods. Although these are proactive measures, further care should be taken in the future to ensure that patient data remains secure.

4. COLLECTION METHODOLOGY

The collection of gait data is the origin of gait analysis upon which all other aspects of gait analysis rely. Poor collection protocols would produce inaccurate gait parameters regardless of the quality of gait data post-processing. There are also considerations to be made at this point about how the data can be collected in a way which is ethical and supportive of the needs of the participant. This section will outline the decisions which were made to produce inertial measurements which will produce actionable gait parameters. The first section will describe the selection of sensor placement locations and describe a method for sensor attachment which will minimize motion artefacts and maintain consistency between trials and participants. The second section will outline the procedure used for collecting the gait data for this project.

4.1. Sensor Positioning and Attachment

The first decision to be made about the gait collection methodology is to decide where to place the IMU sensors. In the literature, foot, shank, thigh, and trunk placements are all common [20]. However, shank and foot are the most effective placement positions for the identification of gait events compared to the thigh and trunk placements according to a review of 17 different gait studies by Panebianco et al. [20]. Some studies use only the foot or only the shank, but in this case both locations were used so that sensor fusion of the two sensor locations could be used to verify gait events. Increasing the number of sensors to include the thigh and trunk could add some data richness at the expense of added complexity in the methodology design and the data analysis. These additional sensors were determined to be unnecessary for this project.

When analyzing gait, it is important to consider the connection between sensor and the body segment to which it is attached. When using any sensor or marker attached to the surface of the skin, some deformation is unavoidable. It is caused by the deformation of the soft tissue surrounding the bone. This results in readings which are not entirely representative of the motion of the bones during gait. It can introduce inertial signals due to oscillation of the sensor following impact. This source of error can be mitigated by attaching sensors in locations where long bones are close to the skin surface. It can also be reduced by taping the sensors either directly to the skin or over tight clothing. Cables should also be taped down to prevent their motion from acting on the IMU sensors. These precautions cannot completely eliminate these motion artefacts, but by minimizing oscillation and understanding when these artefacts will occur, such as on initial contact, it is possible to minimize the effects that these oscillations have on the output data.

One sensor was placed for each body segment, the left foot, right foot, left shank, and right shank. Foot sensors were placed over metatarsals II and III approximately 1 cm from the distal end with the x-axis aligned with the direction of the foot, the same as the direction of walking, rather than the direction of the metatarsals. Shank sensors were placed approximately 30% of the way from ankle to knee with the x-axis of the IMU aligned with the long axis of the tibia pointing downwards toward the ankle joint. Sensors and USB cables were held in place using medical tape. Sensors were taped to tight fitting clothing worn by the subject rather than their own skin to reduce discomfort when removing the tape. This could be adjusted to reduce the effect of deformation or pulling as a result of the tight clothing. Tape was wrapped around the

foot under the arch and the shank tape was wrapped around the whole calf to keep the sensor in line with the body segment and avoid twisting. Figure 2 shows a participant wearing the sensors and carrying the Raspberry Pi 4 computer in the hip pouch. Sensors in this case are all taped firmly over tightly fitted clothing.

Figure 2. Subject wearing the sensor system, the Raspberry Pi computer is inside the hip pouch and the sensors are attached to the shanks and feet, tape is used to secure the sensors and their cables.

4.2. Recommended Gait Data Collection Protocol

The first step in collecting data is to set the data collection rate. Previous packet loss testing has indicated that sampling rates above 250Hz should not be used, because above this sampling rate samples are lost with regularity. For this reason, all gait trials with the FSM-9 should collect at the maximum rate of 250Hz.

Next the participant should be prepared by attaching the sensors as described in the previous section. If an impairment is added to alter the gait pattern it should also be added at this time. This project studied two different patterns of abnormal gait, antalgic gait and limited mobility gait. Antalgic gait was simulated by taping a small plastic object to the underside of the right foot to evoke a painful sensation during the stance phase. Limited mobility gait was simulated by taping a plastic rod to the participants left leg to immobilize the knee joint in an extended position. For both abnormal gait conditions, the participants were asked to walk around briefly to find a comfortable walking strategy to cope with the impairment.

Gait samples were collected for one minute for each trial, with the participant walking at a comfortable speed. Trials were collected under different conditions to test the gait analysis system. These conditions included normal gait, reduced mobility gait, and antalgic gait. Gait trials should be conducted indoors or outdoors on flat ground with no obstacles. Part of the novelty in this device is that enables the collection of gait

data at home or outdoors. It is important when considering a location, that the participant avoid walking near power lines, magnets, large metal objects, or any object which induces a significant magnetic field. These objects could affect the magnetometer used for orientation tracking and may lead to less accurate results.

For the verification of the automated labeling algorithm, participants were asked to follow a right-leg-raised protocol at the start of each trial to assist with the verification of sensor labeling. By raising the right foot at the start of the trial it is possible to use the accelerometer data to reliably match corresponding shank/foot sensors.

Following the gait trial, the gait data was saved to a computer for post-processing. The following chapter goes into detail on the software and algorithms used for the post-processing of gait data in this project.

5. SOFTWARE AND ALGORITHMS FOR OFFLINE PROCESSING

This section will outline the pipeline of data from the moment it is received the sensor to the point where it contains useful gait information such as orientation or trajectory data. Unless otherwise noted, the algorithms were developed by the author. Algorithms were implemented offline in Matlab.

The algorithms for gait analysis provided in this work are meant for off-line implementation. Despite having computational advantage of being run off-line, an attempt was made to implement simple algorithms which could in the future be implemented and run on-line using a microcontroller.

An accompanying program was designed for the controlled use of these algorithms for gait analysis. This Matlab app provides a graphical user interface (GUI) to guide users in their analysis.

5.1. Packet Loss Testing

Packet loss is a result of either failed reading by the sensor or of failed communication between the sensor and the controller. The worst cases of packet loss are when they go unnoticed and the data contains an undetermined number of lost packets inn undetermined locations. In this case the data becomes almost totally unusable. For this reason, the following three metrics, packet loss, packet loss percentage, and relative sampling rate are used as qualifiers for further analysis to take place. Each sensor is tested individually for packet loss to identify any sensor malfunction then the average values are calculated to understand the overall performance of the sensor unit.

Packet loss can be easily diagnosed if the sensor data includes a sequence number. The sequence number is a monotonically increasing integer generated by the sensor each time it means to collect a sample. This allows for the comparison between the theoretical number of packets created by the sensor and the actual number of packets received by the controller. The total number of lost packets is equal to the number of packets created minus the number of packets received.

$$Packet\ Loss = Packets\ Created - Packets\ Received \tag{1}$$

Packet loss percentage is a better metric of data loss because it is relative to the total number of samples sent, so it is comparable between different collection frequencies and durations.

$$Packet\ Loss\ Percentage = \frac{Packets\ Created - Packets\ Recieved}{Packets\ Created} \times 100\% \tag{2}$$

Actual sampling rate is a metric which shows the rate at which samples are created by the sensor. Actual sampling rate is calculated by dividing the number of packets created by the sensor by the duration of elapsed time as measured by the controller's real time clock (RTC).

$$Actual\ Sampling\ Rate = \frac{Packets\ Created}{Time\ Elapsed} \quad (3)$$

Observed sampling rate is a metric designed to ensure that collection is happening at the prescribed sampling rate. Observed sampling rate is calculated by dividing the number of packets received by the duration of elapsed time as measured by the controller's real time clock (RTC).

$$Observed\ Sampling\ Rate = \frac{Packets\ Received}{Time\ Elapsed} \quad (4)$$

5.2. Data Resampling and Trimming

After the data has been qualified for further processing by diagnosing any packet loss the next step is to process the data for further analysis. This includes removing the data header and footer which where sensors are starting up or shutting down. The header size is dependent on the selected sampling rate, because at higher sampling rates the sensor takes a longer time to start up. At the recommended sampling rate of 250Hz the header size is 75 samples or 300ms. The sampling rate is then normalized for all sensors. This is done because each sensor yields a sampling rate which is very slightly different even when no packet loss is identified. Accurate timestamps on every sample allow for the accurate resampling of the data without significant data quality losses. Resampling is done by linearly interpolating sensor data and applying an anti-aliasing filter using the Matlab resample function. Sensor data is then saved to a uniform data structure for each sensor so that it can be simply recalled.

At the end of the collection period sensors turn off in sequence, so some sensors send more samples than others. These excess samples are removed by trimming the ends of the signals to include the same number of samples.

5.3. Automated Sensor Labeling

According to the methodology used there is one sensor on each shank and foot. An algorithm was developed to automatically label each of the sensors ("right shank", left foot", etc.) using their acceleration signals as the input. The flow diagram for this process is shown in Figure 3.

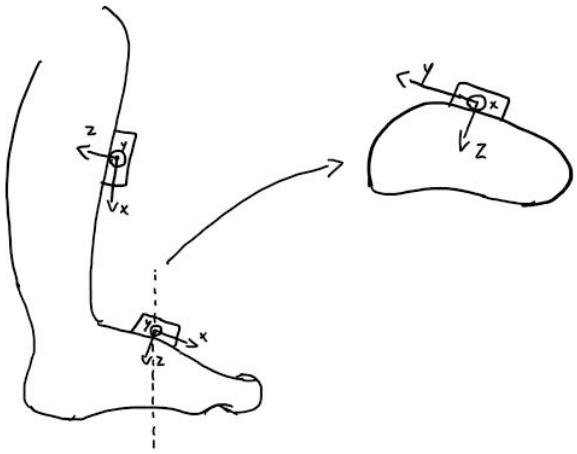

Figure 3. A schematic showing the axes of the shank and foot sensors for the left foot.

The first step of the algorithm differentiates between shank and foot. This is possible by using the z-acceleration signal. The first step is to identify the value of the z-acceleration during the stance phase. During the stance phase the acceleration signal is relatively constant because the foot is in contact with the ground while the other foot progresses forward. This results in the histogram of the acceleration signals having a peak value when the acceleration value is closest to the acceleration value experienced during stance phase, which very similar to the acceleration value when the subject is standing still. During the stance phase the foot sensors have a z-acceleration of approximately -8m/s^2 because the z-axis of the IMU is facing downward, opposite the gravity vector. The shank sensors indicate a z-acceleration near zero because the z-axis is orthogonal to the gravity vector. Histograms for the z-acceleration of a shank and a foot are shown in Figure 4. In this figure it is notable that the shank has a more uniform distribution. This is because, during the stance phase the foot remains static on the ground while the shank continues to move. For this reason, the threshold was selected to be -6m/s^2, slightly closer to the right foot z-acceleration peak. A threshold of -6m/s^2 was used to distinguish between foot and shank sensors.

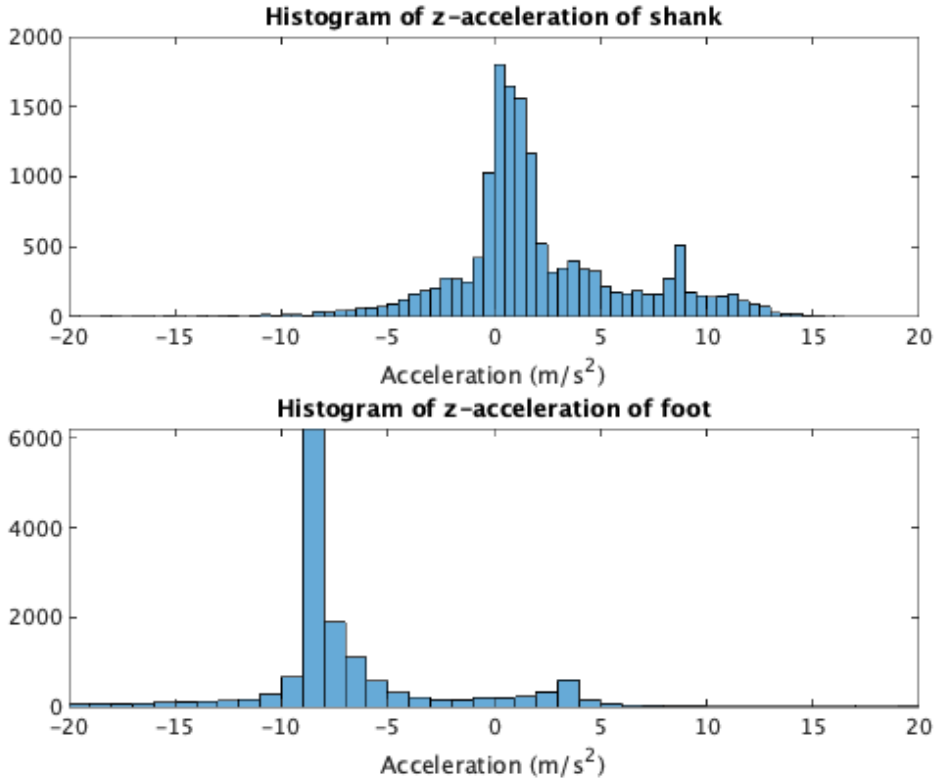

Figure 4. Histograms of z-acceleration for a shank and a foot showing the distribution of acceleration values, which allow for the automated differentiation between foot and shank.

Once the feet and shanks separated the next step is to determine the left and right foot sensors based on the y-acceleration in stance phase. This determination is possible because of the dorsal arch of the foot. Because the sensors are on the outward facing surfaces of the dorsal arch. This causes the y-acceleration vector of the left foot to be slightly positive because it faces slightly upward, and the right foot to be slightly negative, because it faces downward. This is shown in the histograms of left and right feet that are shown in Figure 5. A threshold of 0m/s^2 was used to distinguish between left and right feet.

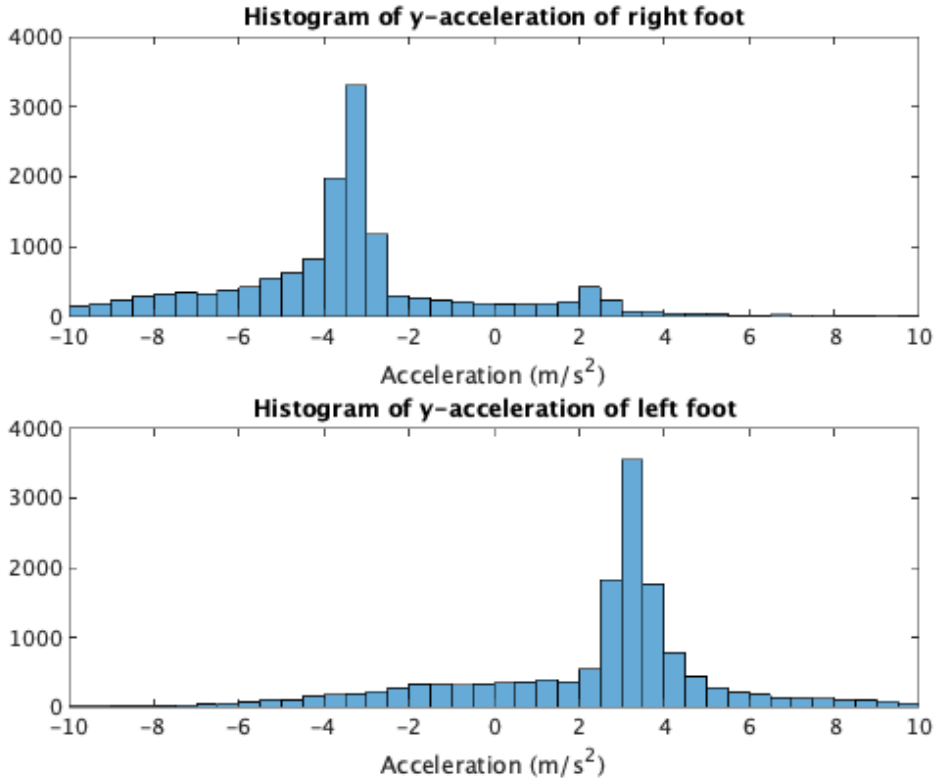

Figure 5. y-acceleration of left and right feet.

Finally, the right and left shank are differentiated by comparing the x-acceleration signals with those of the right and left feet. This works because the impact of the heel strike is detectable in the acceleration signal of shank and foot sensors. The x-acceleration signal was first passed through a 9th order Butterworth high pass filter with a cut-off frequency of 20Hz to isolate the higher frequency acceleration signals found at heel strike. The power of these signals was then found by squaring. Each of the shank power signals are multiplied, elementwise, by the power signal of the left foot. The higher sum of the of the resultant multiplications is the left shank, the lower sum is the right shank. This process is shown in Figure 6, notice how the power signals are aligned for sensors on the same side.

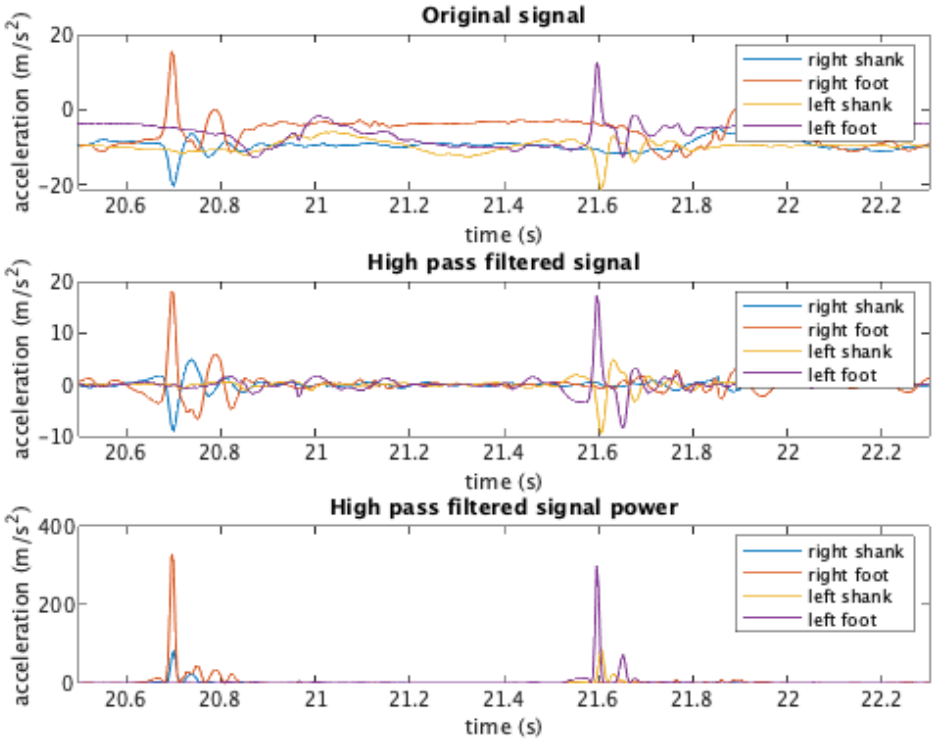

Figure 6. x-acceleration of each sensor before filtering (top), after being passed through a 9th order Butterworth high pass filter with a cutoff of 20Hz (middle), and the power of the filtered signal (bottom).

5.4. Gait Event Detection and Segmentation

Gait events for this thesis were detected according to the four phase model from Taborri et al. [18]. This level of granularity was selected because it offers the ability to investigate the foot roll from heel strike to flat foot. The phases in this model are the loading response, full contact, pre-swing, and swing. In order to identify these phases, the following gait events need to be identified. The four-phase model showing how gait phases are separated by gait events is shown in Table 2.

First, Initial Contact (IC) denotes when the foot first contacts the ground, separating the swing and loading response phases. Loading response then continues until the full contact. The first instant of full contact is the Initial Full Contact (IFC) gait event. The full contact phase continues until the End Full Contact (EFC) event when the heel is first lifted from the ground. EFC marks the beginning of the pre-swing phase which continues until the End Contact (EC) when the whole foot is lifted from the ground. EC marks the beginning of the swing phase which continues until the next IC event.

Table 2. Four phase gait model

Loading Response		Full Contact		Pre-Swing		Swing	
IC		IFC		EFC		EC	IC

The way to segment gait into phases begins with the detection of the IC, IFC, EFC, and EC events. IC and EC events were detected based on an algorithm used by Jasiewicz et al. [19]. The algorithm by Jasiewicz et al. was not used to determine EFC and IFC. The Jasiewicz et al. algorithm identifies search windows for IC and EC events based on local minima and maxima in the angle of ankle plantar flexion [19]. The IC event is identified either as the location of the maxima in z-acceleration or as the zero crossing following the minima in foot angular velocity within the IC search window [19]. The EC event is identified either as the maxima in x-acceleration or by the first peak of foot angular velocity within the EC search window [19]. The proposed algorithm for this work uses a different method for identifying search windows, based on shank angular velocity. After the IC and EC windows are identified, the proposed algorithm is the same as that proposed by Jasiewicz et al for determining EC and IC.

The EC search window is defined for this work as the 250ms before the upward zero crossing of the shank y-axis angular velocity. The IC search window is defined as the 250ms after the downward zero crossing of the shank y-axis angular velocity. The shank signal is advantageous for this purpose, because it only has two zero crossings per cycle, this behaviour is shown in Figure 7. An additional requirement of the proposed algorithm is that the peaks used to find EC and IC must be below a threshold of -130 deg/s.

The location first peak corresponds to the EC event, as outlined in the Jasiewicz et al. algorithm. EFC occurs before EC and is easily identified by the moment where the angular velocity becomes nonzero. For this reason, the EFC event can be found by working backward from the EC event until the value of the angular velocity is sufficiently close to zero (< 5deg/s). The location of the IC and IFC events are found in relation to the second peak. IC is the zero crossing of the foot y-angular velocity preceding the second peak as determined by the Jasiewicz et al. algorithm. IFC is the zero crossing following the second peak. The resultant gait event labels are shown in Figure 7.

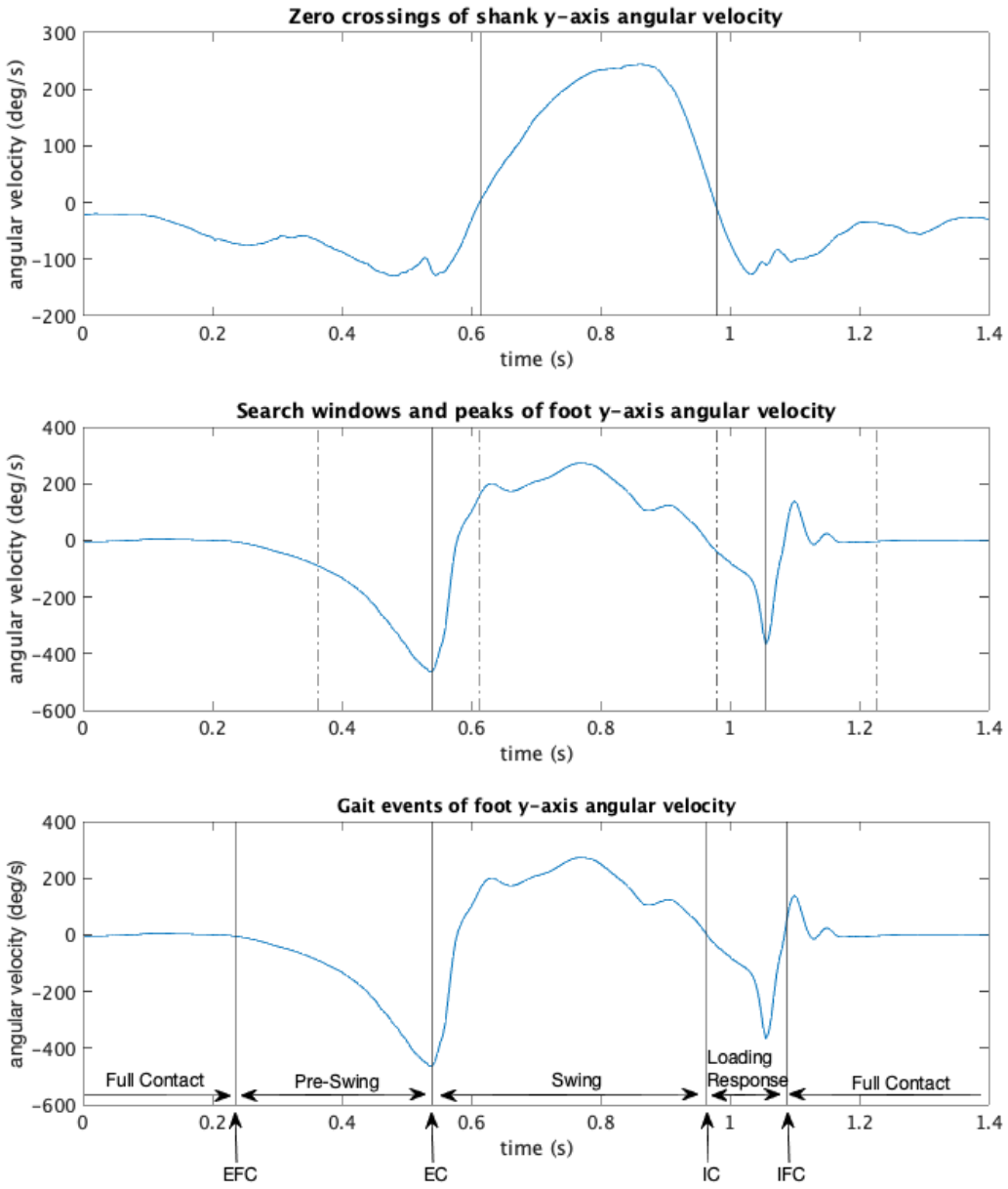

Figure 7. Zero crossings of the shank angular velocity (top), search windows and detected peaks of foot angular velocity (middle), and the resultant gait events and gait phases (bottom).

Now that gait events have been detected, the next step is to remove gait segments that are incomplete or otherwise problematic. This is called the discard step. In this case the segment is defined from one IFC event, to the next EFC event. This is done to ensure that every segment used in the calculation of the gait temporal parameters contains two full contact periods which are used to remove drift due to sensor bias due to drift. This process is discussed in the next section. Figure 8 below shows how gait events are discarded if they do not meet the inclusion criteria. This step is designed to have high specificity to ensure that no artefacts are incorrectly labelled as gait events. First, the algorithm removes all gait events from before the first IFC and after the final EFC. Second, the algorithm checks that all IFC segments are paired up a corresponding EFC segment. This ensures that there are no extra IFC or EFC events in the sample. Third, the algorithm checks the distance between the start of the potential segment,

from one IFC to the next and deletes segments which are more than 1.2 times the mean stride time, from example, the gap between IFC events at 9.5s and 15s in Figure 8. If a long interval like this is detected, all events on the interval are discarded. Finally, the algorithm checks that each potential segment has all the required gait events (IFC, EFC, EC, IC, IFC, EFC), discarding segment that either do not have all events or have events occurring in the wrong order.

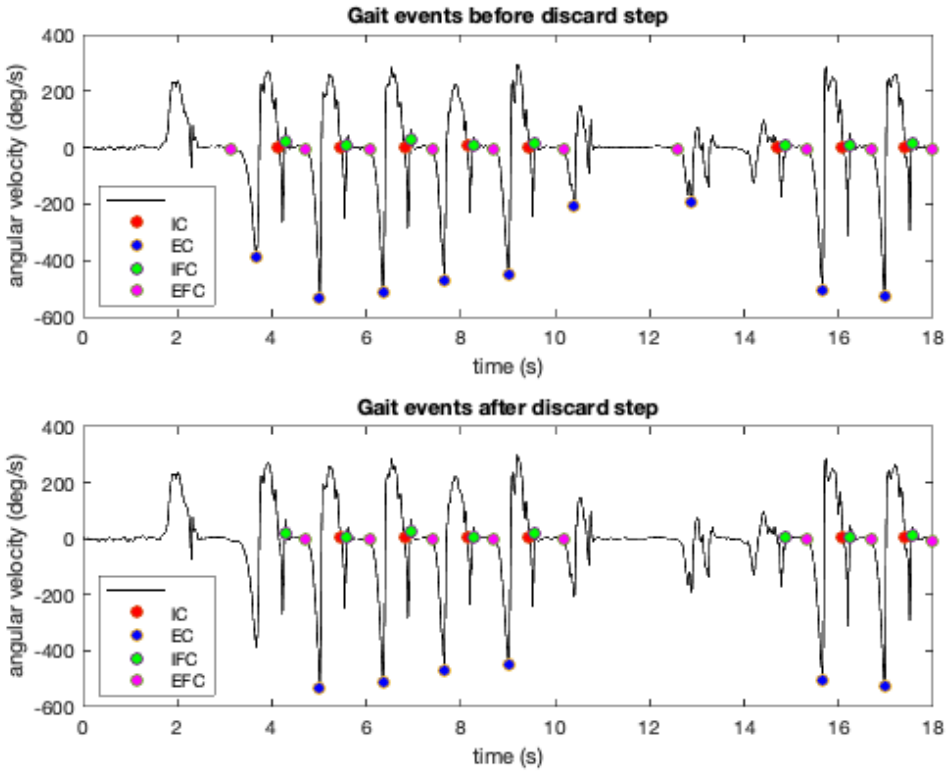

Figure 8. Foot y-axis angular velocity with gait event labels before and after gait segment discard step.

5.5. Gait Temporal Parameters (GTP)

Gait temporal parameters (GTP) are important manifestations of gait patterns. Different GTP can indicate differences in gait patterns between legs, between trials, or between populations. The most common GTP are stride time, cadence (which is the inverse of stride time), stance time, swing time, stance percentage, and swing percentage. Stride time is defined as the time from one initial contact to the next (5). Cadence is the inverse of stride time multiplied by 60 to get strides/min (6). Stance time is the time from initial contact to the next end contact (7). Swing time is the time from one end contact to the next initial contact (8). Stance percentage is the percentage of the stride in which the foot is on the ground (9). Swing percentage is the percentage of the stride in which the foot is off the ground (10)

$$Stride\ Time = IC_{k+1} - IC_k \quad (5)$$

$$Cadence = \frac{60}{Stride\ Time} \tag{6}$$

$$Stance\ Time = EC_{k+1} - IC_k \tag{7}$$

$$Swing\ Time = IC_k - EC_k \tag{8}$$

$$Stance\ Percentage = 100\% * \frac{Stance\ Time}{Stride\ Time} \tag{9}$$

$$Swing\ Percentage = 100\% * \frac{Swing\ Time}{Stride\ Time} \tag{10}$$

Symmetry ratio (SR) is the final gait temporal parameter mentioned here. SR is unique in that it can be applied to any parameter of gait that is measured in the same way for both left and right sides, it provides a measure of how similar the gait parameters are for each side. It is found by dividing the left side GTP by the same GTP on the right side to get a value of 1 for perfect symmetry (11).

$$Symmetry\ Ratio = \frac{Left}{Right} \tag{11}$$

Gait temporal parameters are calculated for each stride in the sample and then averaged. The mean GTP values shown are calculated for all strides in the sample. Table 3 below shows a series of GTP for normal gait.

Table 3. Gait temporal parameters of a typical sample of normal gait

	Left Mean	Right Mean	Symmetry
Stride Time (s)	1.771	1.788	0.991
Cadence (strides/min)	33.974	33.639	1.010
Stance Time (s)	1.104	1.141	0.968
Swing Time (s)	0.667	0.647	1.030
Stance Percent (%)	62.258	63.715	0.977
Swing Percent (%)	37.742	36.285	1.040

5.6. Foot Orientation and Position Tracking

Foot orientation and position tracking are ideal measurements, because they can be easily visualized and interpreted. They also provide some unique and insightful gait parameters which will be discussed. Together, these measurements show the trajectory of the foot throughout the gait cycle. These measurements are recalculated for each

iteration of the gait cycle. For simple interpretation, it is ideal to obtain these measurements relative to some known frame. For this project, the known frame is the ground frame (∑G) where the z-axis is pointed upward, orthogonal to the ground, x-axis is parallel to the ground in the direction of walking, and y-axis is orthogonal to x and z axes. This is shown in Figure 9. The position of this reference is defined as relative to the initial position of the foot during full contact for each stance phase. The algorithms used in this section to calculate orientation and position are based on those used in a paper by Kitagawa and Ogihara [26].

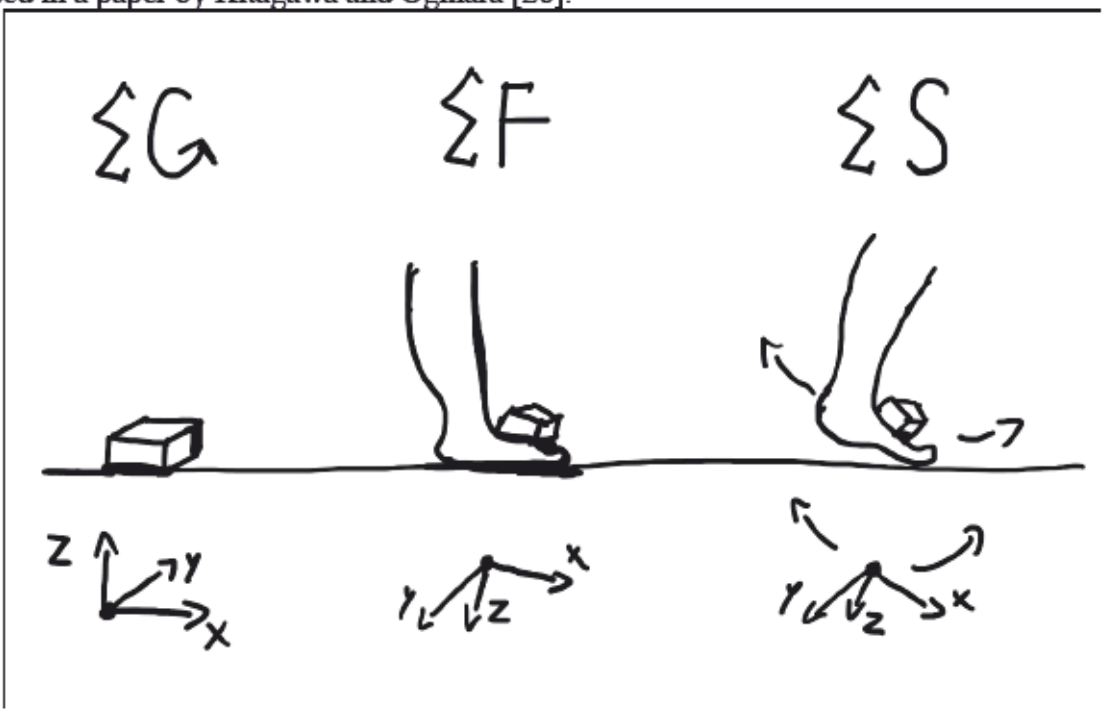

Figure 9. Orientation of ground frame (∑G), full contact frame (∑F), and sensor frame (∑S). Note that ground frame and full contact frame are static, while sensor moves throughout the gait segment.

The Hillcrest FSM-9 IMU used for this project automatically measures sensor orientation relative to initial sensor orientation. This frame, relative to the initial sensor orientation is the sensor frame (∑S). In order to get the orientation in to the ground frame it is necessary to find a frame that is consistent between segments. This is the full contact frame (∑F). The full contact frame is represented by the orientation of the sensor when the foot is in the foot is in the full contact phase. Because the foot returns to this position each stride, it is consistent between orientations. The transformation from ∑S to ∑F is done by dividing the quaternion array describing the sensor-based orientation piecewise by the single quaternion describing the orientation 75% of the way through the full contact phase represented by t_0. Note that for the purpose of representation, quaternions are depicted by rotations, where subscripts represent the initial frame and superscripts represent the destination frame. However, in the programming, quaternion rotations were used whenever possible to avoid gimbal lock. In the following equations a represents the linear acceleration. Superscripts are used to denote the frame in which the vector is represented.

$$^{F}R_S(t) = R_S(t)\,[R_S(t_0)]^T \tag{12}$$

The rotation matrix ${}^{F}R_S(t)$ can be broken down into its constituent rotations about each axis described by i, j, and k.

$$[i\ j\ k] = {}^{F}R_S(t) \tag{13}$$

The rotation ${}^{F}R_S(t)$ is used to determine pronation and in-turn. These measurements are based on the roll, α, and yaw, γ, of the rotation matrix ${}^{F}R_S(t)$. These two measurements could be useful in monitoring for abnormal walking patterns. Pronation is defined as the inward rotation of the foot about the x-axis. In-turn is the inward rotation of the foot about the z-axis. Note that for the left foot these are indicated by positive roll and yaw values, with on the right foot they are indicated by negative roll and yaw values. The equations for pronation angle, $\theta_P(t)$ and in-turn angle, $\theta_I(t)$. Are shown in equations 13 and 14 below.

$$\theta_P(t) = \begin{cases} \alpha(t), & left\ foot \\ -\alpha(t), & right\ foot \end{cases} \tag{14}$$

$$\theta_I(t) = \begin{cases} \gamma(t), & left\ foot \\ -\gamma(t), & right\ foot \end{cases} \tag{15}$$

The rotation ${}^{F}R_S(t)$ is then used to rotate acceleration vectors into the flat foot reference frame.

$${}^{F}a(t) = {}^{F}R_S(t)\ {}^{S}a(t) \tag{16}$$

$${}^{F}\bar{a}(t) = {}^{F}a(t) - {}^{F}a(t_0) \tag{17}$$

The next important issue is to find the rotation which transforms the ∑F to ∑G. This was found using the known direction of acceleration due to gravity, orthogonal to the ground, and the assumption that the sensor was positioned correctly to have the x-axis of the sensor pointing in the direction of walking, in the sagittal plane of the foot. With these assumptions the rotation from ∑F to ∑G was found using the following equations.

$$z = \frac{{}^{F}a(t_0)}{\left|{}^{F}a(t_0)\right|} \tag{18}$$

$$y = \frac{z \times i}{|z \times i|} \tag{19}$$

$$x = y \times z \tag{20}$$

$$^{F}R_{G} = [xyz] \tag{21}$$

The orientation relative to the ground position can then be described by $^{G}R_{S}(t)$. This quaternion can be represented as a rotation matrix or as Euler angles for demonstration purposes. The Hillcrest sensor determines orientation through the integration of angular velocity fused with the knowledge of the direction of the gravity vector from the accelerometer and the direction of the greatest magnetic field strength from the magnetometer. Orientation errors were further corrected by correcting for sensor drift by assuming the sensor would return to the same orientation during each full contact phase.

$$^{G}R_{F} = \left[^{F}R_{G}\right]^{T} \tag{22}$$

$$^{G}R_{S}(t) = {}^{G}R_{F}\,{}^{F}R_{S}(t) \tag{23}$$

The linear acceleration vector relative to the ground frame can then be found by applying the frame rotation $^{G}R_{F}$ to the acceleration without gravity $^{F}\bar{a}(t)$.

$$^{G}\bar{a}(t) = {}^{G}R_{F}\;{}^{F}\bar{a}(t) \tag{24}$$

The acceleration without gravity is then integrated using the trapezoid rule to get linear velocity. Integration can be problematic because it can quickly introduce errors caused by sensor bias, which grow continuously and unpredictably. This was managed in two different ways. First, acceleration data was filtered using a 9th order Butterworth low-pass filter with a cut-off frequency of 20Hz. This cut-off was chosen, because it is high enough to not affect the frequencies typical of human gait, while remove large amounts of accelerometer noise which could increase integration error. The next way in which integration error was mitigated was by making assumptions about foot velocity and foot position at each full contact phase.

Velocity was calculated by integrating the acceleration without gravity signal from IFC to the following EFC event. Leaving in two phases of full contact, before and after the swing phase to use for drift compensation. The assumption was made that velocity in all directions would be zero during each phase of full contact. This is logical, because at each full contact phase the foot remains planted on the ground while the other foot swings past. This assumption allows for the interpolation of drift error for each signal which can then be subtracted from the original for each segment. The amount of drift for each point in each of the phases was therefore set to be the same as the calculated value of velocity for that point. To estimate the amount of drift during pre-swing, swing, and loading response the drift was linearly interpolated between the two full contact phases. This is shown by the example of z-velocity of the foot in Figure 10 below.

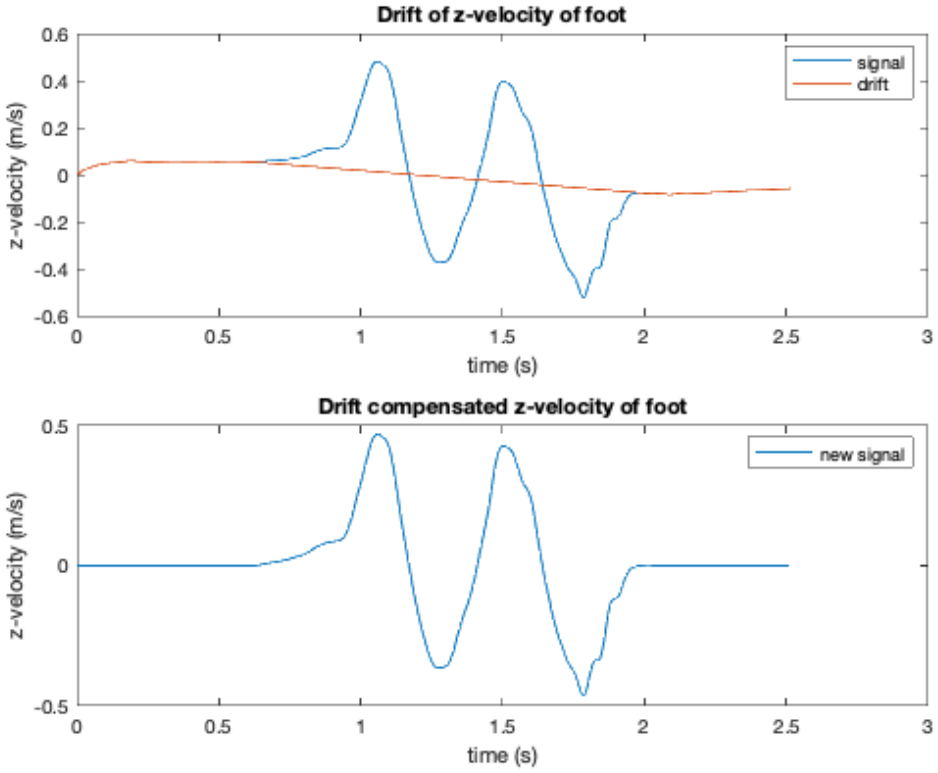

Figure 10. Drift and linear drift compensation for one segment of normal gait.

Similarly, position was calculated by integrating velocity over the same interval. In the case of position, the x and y values cannot be assumed to be constant between phases of full contact, because the foot is landing in a different position than where it left the ground. However, if the gait is occurring on a flat surface, as in this project, the change in z-position from one full contact to the next can be assumed to be zero. This is very helpful, because it removes integration error from the measurement of the height from the ground during walking with is incredibly useful for producing measurements such as foot clearance during walking. In this case a spline interpolation was used, because it seemed to best represent the sensor drift found during the integration. This drift compensation for z-position is shown below in Figure 11 for a representative gait segment.

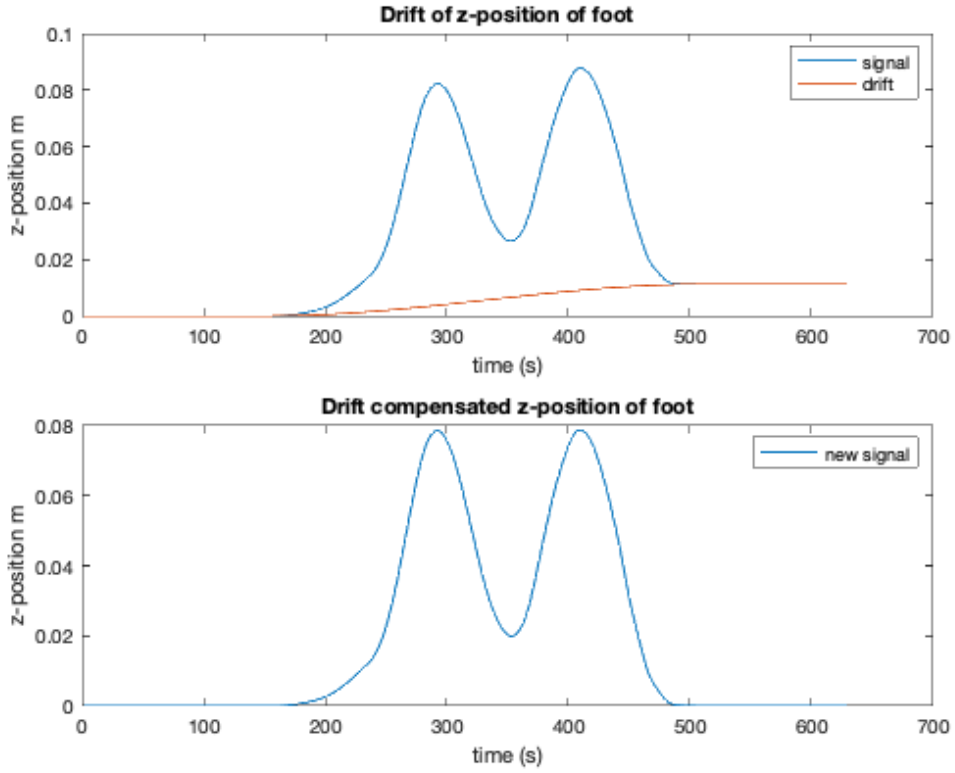

Figure 11. Drift and spline drift compensation for one segment of normal gait.

This measurement of foot position for each step allows for the extraction of four important gait position parameters, step length (SL), foot clearance 1 (FC1), foot clearance 2 (FC2), and minimum foot clearance (MFC). SL is simply the x-position change from one full contact phase to the next, FC1 and FC2 are the peak heights of the position curve shown in Figure 12, and MFC is the minimum point between the two peaks. Figure 12 shows how these are found based on the trajectory plot for a single stride of normal walking. These values were then averaged for all strides in the sample to get the position parameters of the sample. An example of these position parameters is shown in Table 4 below.

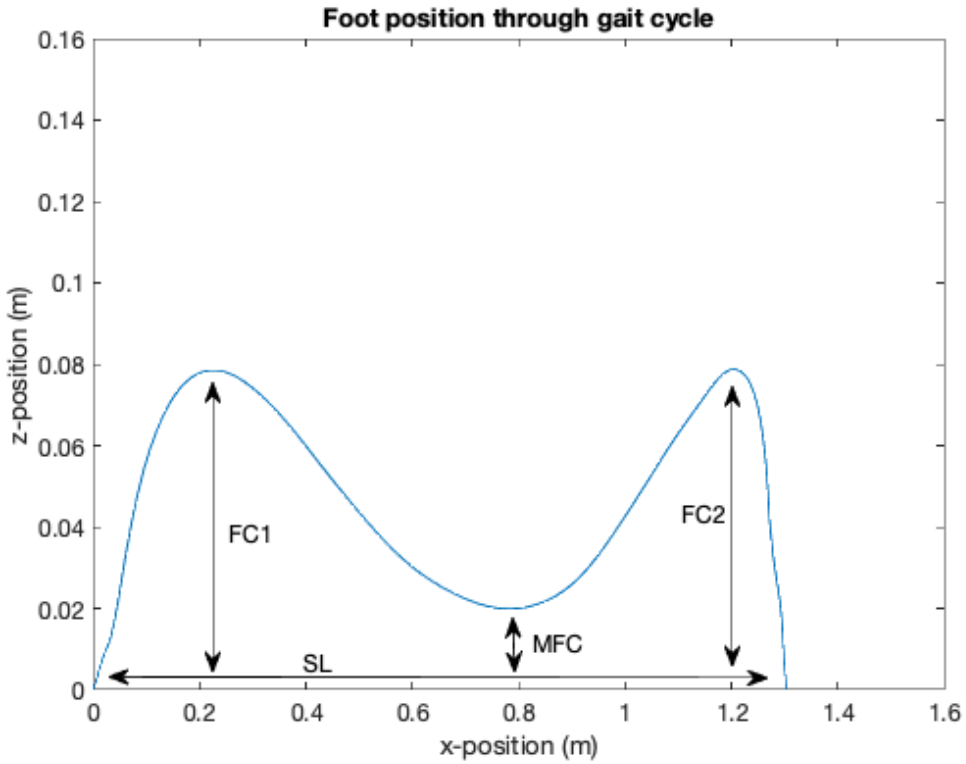

Figure 12. Trajectory of x and z position of foot through a normal gait cycle, showing how FC1, FC2, MFC, and SL are found.

Table 4. Example of position parameters for normal gait

	Left Mean	Right Mean	Symmetry
Foot Clearance 1 (m)	0.061	0.070	0.871
Foot Clearance 2 (m)	0.047	0.078	0.604
Minimum Foot Clearance (m)	0.203	0.231	0.878
Step Length (m)	1.220	1.300	0.938

6. RESULTS

This chapter goes into detail on the results of testing the gait analysis system. This begins with an analysis of the packet loss for the sensor unit. The following sections show results from the various algorithms used in this project for automated sensor labelling, gait segmentation, trajectory tracking, and calculation of gait parameters.

6.1. Packet Loss Testing

Packet loss was tested for the three highest sampling rates for the hillcrest sensors, 250Hz, 333Hz, and 500Hz. This was done to determine the highest feasible sampling rate. Note this is the only test in which sampling rates above 250Hz were used. Higher sampling rates were not used in actual gait trials, because of the packet loss that was found to occur.

At 250Hz, there were no packets lost in any of the sensors. This is the perfect scenario, where the sampling rate works out the desired rate without unknowingly missing out on any data points. This was tested for three times for the exclusive purpose of packet loss testing. Packet loss data was also collected for every gait trial. In all cases, no packet loss occurred. Table 5 below shows a representative sample of packet loss characteristics for a 30 second collection period. The following Tables 6 and 7 show the results from representative samples collected at 333Hz and 500Hz respectively.

Table 5. Packet loss of sensor unit at 250Hz

	Packets Received	Packets Lost	Percentage Lost (%)	Collection Duration (s)	Actual Sampling Rate (Hz)	Observed Sampling Rate (Hz)
Sensor1	7467	0	0	29.84	250.25	250.25
Sensor2	7447	0	0	29.83	249.61	249.61
Sensor3	7468	0	0	29.84	250.28	250.28
Sensor4	7459	0	0	29.84	249.98	249.98

Table 6. Packet loss of sensor unit at 333Hz

	Packets Received	Packets Lost	Percentage Lost (%)	Collection Duration (s)	Actual Sampling Rate (Hz)	Observed Sampling Rate (Hz)
Sensor1	9927	36	0.36	29.87	333.61	332.41
Sensor2	9905	33	0.33	29.86	332.80	331.69
Sensor3	9935	30	0.30	29.86	333.68	332.68
Sensor4	9923	30	0.30	29.86	333.28	332.27

Table 7. Packet loss of sensor unit at 500Hz

	Packets Received	Packets Lost	Percentage Lost (%)	Collection Duration (s)	Actual Sampling Rate (Hz)	Observed Sampling Rate (Hz)
Sensor1	9340	5224	35.87	29.29	497.29	318.92
Sensor2	10697	3933	26.88	29.44	496.96	363.36
Sensor3	8422	6141	42.17	29.25	497.87	287.92
Sensor4	8914	5589	38.54	29.24	495.92	304.81

It is visible from these tables that packet loss becomes a slight issue when sampled at 333Hz and a significant problem at 500Hz. At 333Hz only ~0.3% of samples were lost making the observed sampling rate only slightly lower than 333Hz. Because it is known which samples are missing, one could simply interpolate over the missing samples, provided they do not all occur consecutively. Lost packets are distributed relatively equally over the four sensors. At 500Hz there is a much higher rate of loss of 25-45% making up a significant portion of the signal. Lost packets in this sample were not similar across sensors suggesting and often occurring consecutively, reducing the efficacy of using interpolation to compensate for lost packets. The observed sampling rates at a selected rate of 500Hz are also less than the observed sampling rates at a selected rate of 333Hz for 3 of 4 sensors.

6.2. Automated Sensor Labeling

The automated sensor labeling is an important feature of this project. If sensors are labeled incorrectly it would prevent the following algorithms from functioning properly and could result in inaccurate gait outputs. Luckily, it is relatively simple to judge if the algorithm is working by investigating the accelerometer data for each of the gait samples. The verification of this algorithm is made possible by the right-foot-raised protocol in which the participant is asked to begin the trial standing upright with their knee flexed. In this position we can reliably identify each different sensor by its accelerometer signal due to the known acceleration vector due to gravity. Table 8 below shows the axis (x, y, or z) and the direction (+ or -) with which the gravity vector is most closely aligned for each sensor in each case.

Table 8. Approximate direction of gravity vector while at rest for right-foot-raised and normal stance position during gait

	Right Foot Raised (Initial)	Stance Phase (During Gait)
Left Foot	-z	-z
Left Shank	-x	-x
Right Foot	-x	-z
Right Shank	+z	-x

Figure 13 shows sensor acceleration values in the x, y, and z axes for the first 15 seconds of a normal gait sample where the right-foot-raised protocol was followed for the first ~7 seconds. The labels shown in the legend were provided by the sensor labelling algorithm and can be validated by observation.

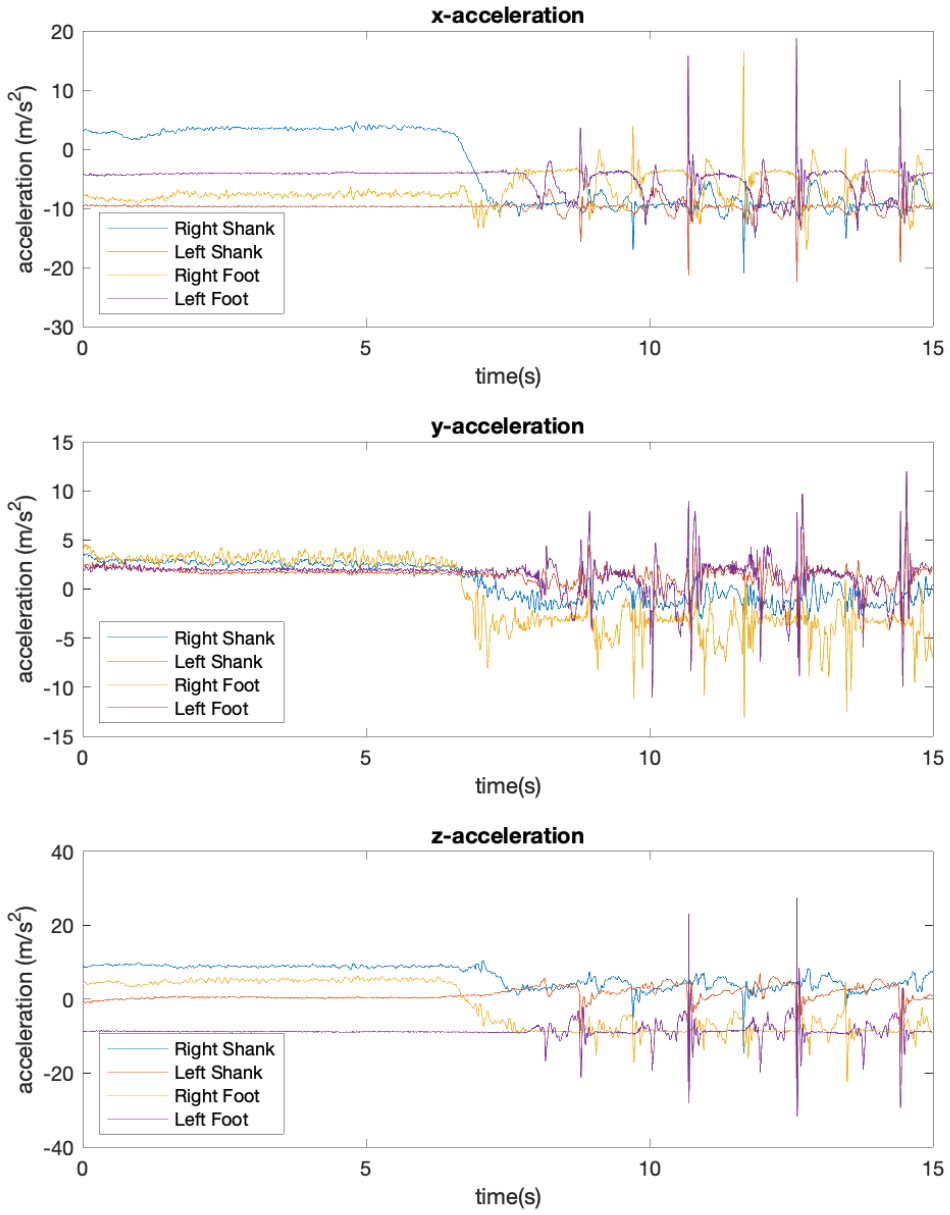

Figure 13. Acceleration of each sensor for first 15 seconds of normal gait trial incorporating the right foot raised protocol.

As expected, the right shank z-axis aligns with the gravity vector when the right foot is raised, indicated by a z-acceleration of ~9m/s^2 for the first 7 seconds when the foot is raised. Then during stance phase the x-axis aligns opposite the gravity vector indicated by the x-acceleration of ~-9m/s^2 for the remainder of the sample. The right foot also undergoes changes from having x-acceleration values of ~-9m/s^2 for the first 7 seconds to having the gravity vector shift to the z-axis as the x-acceleration gets closer to zero and the z-acceleration gets closer to -9m/s^2. The left shank and foot are not raised at any point, so they are expected to remain the same over the collection

duration. The shank has an x-acceleration of ~-9m/s^2 while the left foot has an z-acceleration of ~-9m/s^2.

For this sample and all other samples tested, the results were the same. In all cases the labeling by the algorithm produced the same results as labeling by observation. This is somewhat expected because the algorithm was built based on the walking patterns of the two individuals whose gait was collected. The labelling algorithm did work for the simulated cases of antalgic gait and limited mobility gait, which indicates that the labeling algorithm could be widely applicable to different styles of gait.

6.3. Gait Event Detection and Segmentation

When determining the effectiveness of the gait segmentation algorithm, two key questions come to mind. First, does the algorithm correctly identify the temporal location of gait events? Second, does the algorithm correctly identify full stride segments while discarding artefacts?

Gait segmentation was completed using the gait segmentation algorithm presented in section 5.4. Gait segmentation was done for all different simulated gait styles and was successful in detecting gait events in each of them. This was found by comparing the results of the algorithm to an alternative algorithm for detecting EC and IC events defined in the same paper by Jasiesicz et al. which was used as a basis for the proposed algorithm for gait event detection based on foot angular velocity.

According to a Jasiewicz et al., x-acceleration and z-acceleration can also be used to determine gait event locations [19]. The study shows that the EC event corresponds with the first peak of x-acceleration within the EC search window which follows the flat sections indicative of the full contact phase. The study also shows that the IC event corresponds with the last positive peak in z-acceleration within the IC window prior to the full contact phase.

Figure 14 shows an example of how the segmentation accurately captures gait events by comparing the detected gait events locations to the z and x axis accelerations of the foot. This figure is significant, because it compares the results to an alternative method of detecting gait events, which is to detect peaks in z and x foot acceleration.

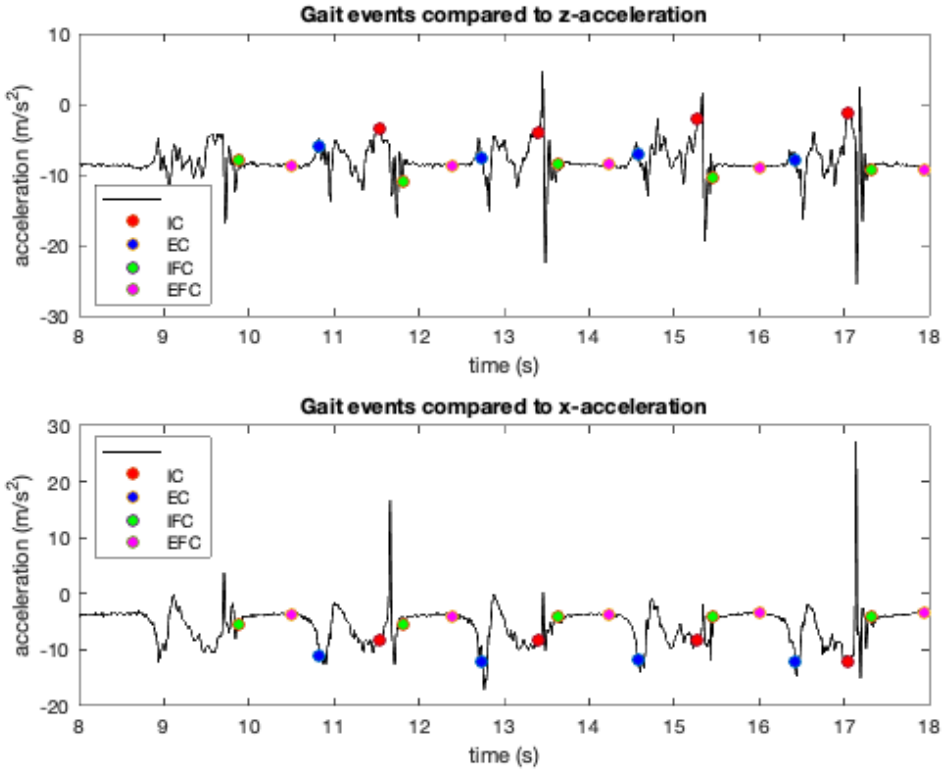

Figure 14. Gait events compared to foot acceleration for a representative sample of normal gait.

By observing Figure 14 it is visible that the EC events, identified by the blue dots, are found, as expected, on the x-acceleration peaks following the full contact gait phase. Likewise, the IC events, identified by the red dots, are found, as expected, on the z-acceleration peaks preceding the full contact gait phase. The EFC events also seem accurate based on the x-acceleration, because the EFC location is detected at the moment that the x-acceleration leaves the steady state of the full contact phase. There is some deviation in the location of the IFC events. IFC events in Figure 14 show the IFC event occurring while the sensor is still experiencing acceleration in both x and z axes.

Any potential differences in the calculation of gait events between methods appear very small. This verification by an alternative method supports that the algorithm provided in this thesis which detects gait event locations based on angular velocity of the shank and foot sensors is effective in accurately identifying the temporal location of gait events.

The following Figure 15 shows two examples of gait, one which is continuous and the other which is continuously stopping and starting. This is down to demonstrate the samples that are lost in the discard step. In this figure, the maintained stride segments are green, and the discarded segments are red.

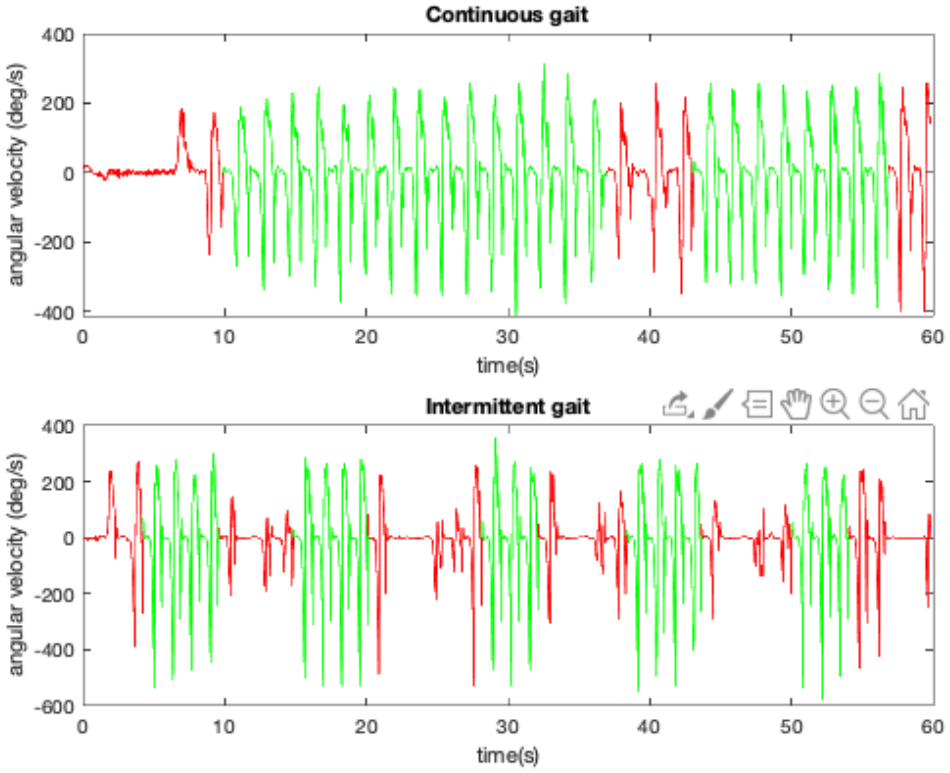

Figure 15. Discarded and maintained stride segments for continuous and intermittent gait, maintained segments are shown in green, discarded segments are shown in red.

It is visible from Figure 15 that the algorithm acts as intended, with high specificity, to ensure that no artefacts that resemble a gait cycle are recorded, at the cost of discarding some true gait segments. Artefacts around 26s in the in the intermittent gait section of Figure 15 show the benefit of how artefacts are discarded and not mistaken for true gait segments. Gait segments around 40s in the continuous gait sample show how some true gait cycle segments are unintentionally removed.

6.4. Gait Temporal Parameters

The tables below show gait temporal parameters for normal, antalgic, and limited mobility gait. These were calculated based on the calculations shown in section 5.5. Each table shows the mean GTP for a single, representative 60 second sample of gait data. Each sample will be analyzed to show the differences in GTP between the three kinds of gait

Table 9 shows the GTP of normal gait. This can be considered a baseline when looking at the other tables. It is shown that the participant takes one stride, or two steps, every 1.8 seconds. The stance and swing phase times are very similar for the left and right feet and therefore have symmetry values which are very close to one.

Table 9. Gait temporal parameters for a sample of normal gait

	Left Mean	Right Mean	Symmetry
Stride Time (s)	1.771	1.788	0.991
Cadence (strides/min)	33.974	33.639	1.010
Stance Time (s)	1.104	1.141	0.968
Swing Time (s)	0.667	0.647	1.030
Stance Percent (%)	62.258	63.715	0.977
Swing Percent (%)	37.742	36.285	1.040

Table 10 shows the GTP for a sample of antalgic gait, caused by a painful sensation in the right foot while walking. The first note is that the stride times have decreased meaning that more steps are being be second compared to normal walking. This could be a result of trying to compensate for smaller steps by increasing cadence to walk at a normal speed. Another noticeable change is the symmetry values for stance and swing features which fluctuate farther from zero. Upon investigation of the stance and swing parameters it becomes evident that this is due to a relative increase in stance percentage for the left foot and a corresponding increase in swing percentage for the right foot. This appears to be a logical result as the participant would want to avoid the painful sensation of bearing weight on the right foot and therefore compensates by having a shorter right stance phase.

Table 10. Gait temporal parameters for a sample of antalgic gait which was simulated by taping a small plastic object to the underside of the right foot

	Left Mean	Right Mean	Symmetry
Stride Time (s)	1.537	1.555	0.988
Cadence (strides/min)	39.080	38.637	1.011
Stance Time (s)	1.016	0.943	1.077
Swing Time (s)	0.520	0.611	0.851
Stance Percent (%)	66.126	60.649	1.090
Swing Percent (%)	33.874	39.351	0.861

Table 11 shows the GTP for a sample of limited mobility gait, caused by having the left knee joint immobilized in an extended position. The first note is that similar to the antalgic gait, there is an increase in cadence from the normal walking sample. There are also significant differences in the stance and swing parameters. The stance percentage of the left foot is significantly decreased compared to normal while the stance percentage of the right foot is increased. These changes result in symmetry values which are farther from 1. This decrease in stance percentage is logical because with the left knee immobilized it would be more difficult to maintain balance while the right foot is in swing phase, incentivizing the participant to reduce the amount of time that the right foot is in swing phase.

Table 11. Gait temporal parameters for a sample of limited mobility gait which was simulated by immobilizing the left knee joint in an extended position

	Left Mean	Right Mean	Symmetry
Stride Time (s)	1.527	1.517	1.007
Cadence (strides/min)	39.352	39.584	0.994
Stance Time (s)	0.814	1.019	0.799
Swing Time (s)	0.713	0.498	1.431
Stance Percent (%)	53.294	67.161	0.794
Swing Percent (%)	46.706	32.839	1.422

These tables of gait temporal parameters show how the abnormal styles of gait can be identified based on temporal changes in the occurrence of gait events. Further understanding of gait abnormalities can be understood by tracking changes in orientation and position throughout the gait cycle. These changes will be explored in the following section.

6.5. Foot Orientation and Position Tracking

The methods shown in section 5.6 were used to find the orientation and position of each foot sensor throughout the gait cycle. These findings are demonstrated below for each type of gait, normal gait, antalgic gait, and limited mobility gait. Results for each gait type are represented with 3 figures and 1 table. The first figure shows the patterns of foot pronation and in-turn for the sample. The second figure shows the patterns of x and z position throughout the gait cycle. Both of these figures are plotted with respect to the percent of the gait cycle with 0% being the IFC event and 100% being the next IFC event. The sections after 100% to show the transient behaviour of the sensor as it comes to rest after the second IFC event, even though this is technically part of the next gait cycle. The third figure shows the x and z position trajectory of the foot through the gait cycle. Finally, the table shows the accumulated gait parameters which are calculated based on the orientation and position of the foot sensors.

The pronation and in-turn of the normal gait sample shown in Figure 16 indicate little pronation during the stance phase and negative pronation (supination) during the swing phase. This is logical because as the foot rolls off of the toes the foot twists to promote clearance for the toes to lift off the ground resulting in both supination and in-turn. Note that for each leg, shown separately in red or blue, the peak supination and in-turn occur at the same time around the time of EC. Interestingly, these occur at different times in the gait cycle for this individual, showing the highly personal quality of data, even for normal gait. Another interesting feature is that the right foot experiences a much lower angle of supination compared to the right foot.

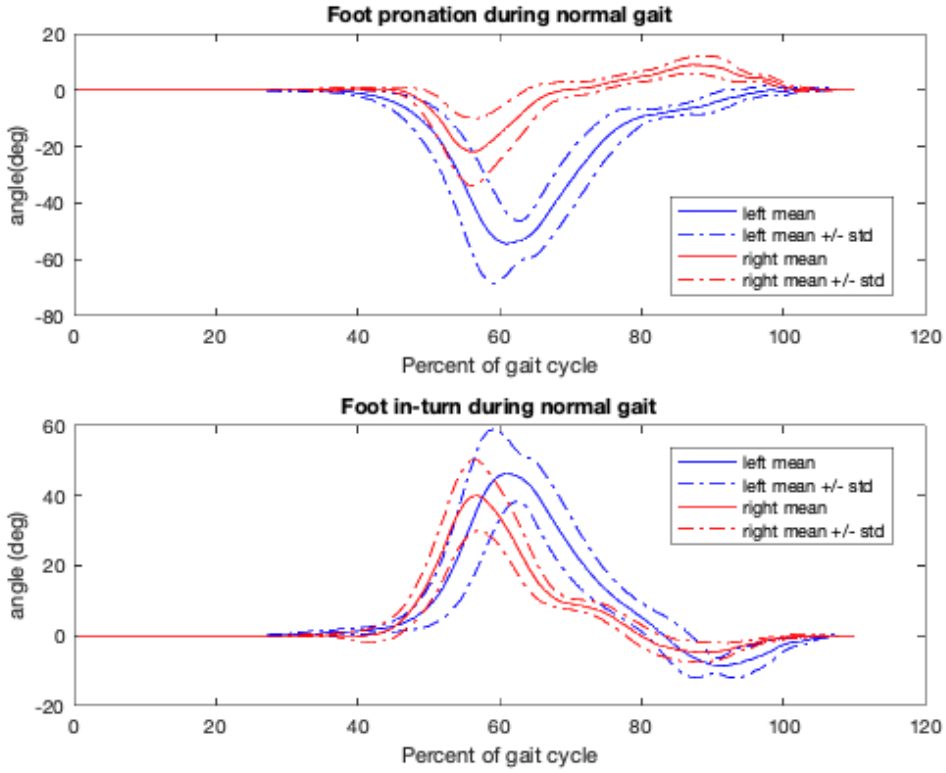

Figure 16. Foot pronation and in-turn for a sample of normal gait.

The x and z positions of the foot for normal walking are shown in Figure 17. From this figure it is noticeable that the x displacement shown by the final value of x-position is on average higher for the right foot than the left. The standard deviation for each step appears similar between the two feet. For z-position there are some more noticeable differences. Although the first peaks of z-position are similar between right and left, the left foot has a significantly lower second peak compared to the right foot

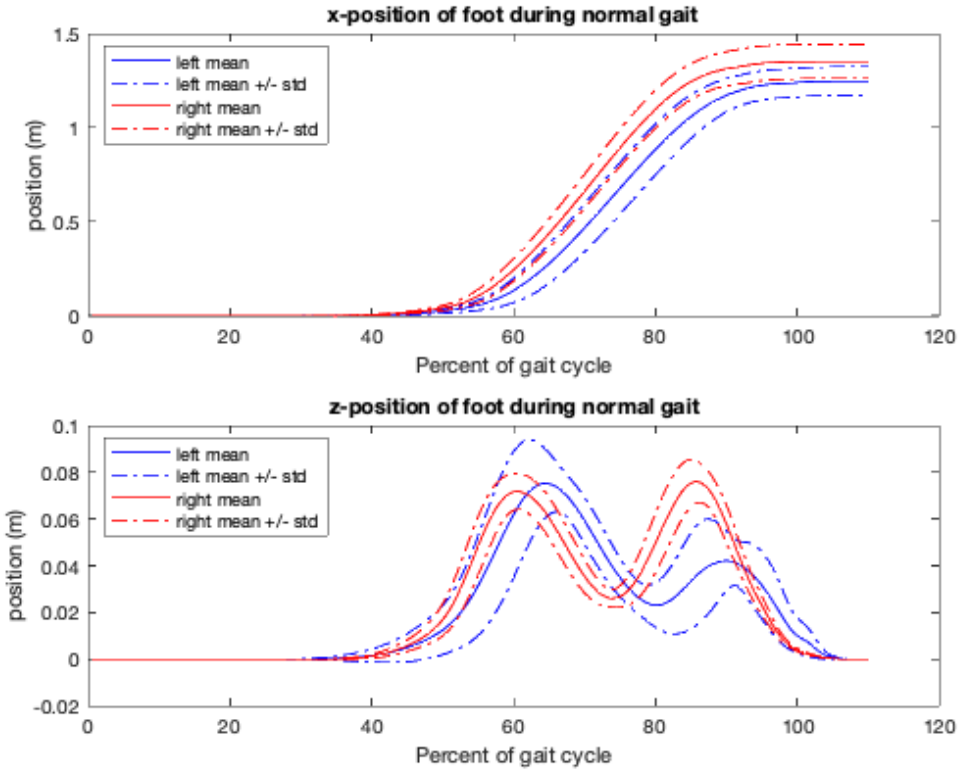

Figure 17. x and z position of foot for a sample of normal gait.

The x and z position trajectory shown in Figure 18 contains very similar information to the figure above. It shows the significantly shorter step length and lower second foot clearance of the left foot compared to the right.

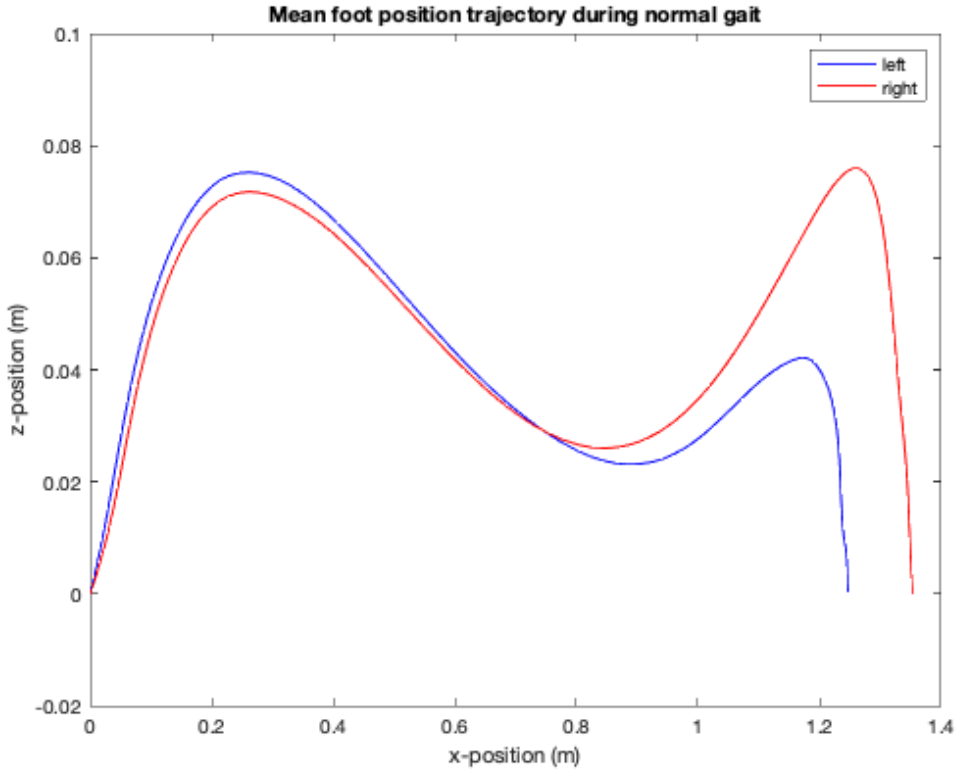

Figure 18. x and z position trajectory for a sample of normal gait.

The table of orientation and position parameters for normal walking shown below shows the orientation and position parameters for a sample of normal gait. Effectively this table summarizes some features which are evident through inspection of the previous three figures. For example, the lower min pronation angle of the left foot shows that there is significantly more supination in the left foot compared to the right. It also shows a higher maximum value of pronation in the right foot compared to the left. The similarity in in-turn between samples is shown by the similar max an min values between left and right. Additionally, it shows similar values for the first foot clearance peak with lower values in the left foot for the second foot clearance peak. This difference is also visible in the symmetry value of the second foot clearance. Finally, it is shown that the mean step length is slightly longer for the right foot compared to the left.

Table 12. Table of orientation and position parameters for a sample of normal gait

	Left Mean	Right Mean	Symmetry
Max Pronation (deg)	1.509	9.595	0.157
Min Pronation (deg)	-63.676	-24.326	2.618
Max In-Turn (deg)	54.530	42.472	1.284
Min In-Turn (deg)	-12.066	-5.728	2.106
Foot Clearance 1 (m)	0.082	0.073	1.114
Foot Clearance 2 (m)	0.053	0.078	0.687
Min Foot Clearance (m)	0.020	0.025	0.790
Step Length (m)	1.247	1.353	0.922

The following figures and tables demonstrate antalgic gait. The Figure 19 shows how antalgic gait changes the pattern of foot pronation and in-turn. The right foot which experiences the painful sensation while in stance shows most of the changes. First, the right foot does not supinate even slightly like in the normal trials, instead it undergoes further pronation during the swing phase. However, it is unclear if this is actual pronation or if the foot in stance phase was simply much more supinated than normal to avoid the painful sensation. This uncertainty shows one potential issue with the decision to assume a normal flat foot position during each stance phase. In terms of in-turn the peak in-turn of the right foot also decreases significantly, this could also be due to the assumption of the flat foot position during stance phase.

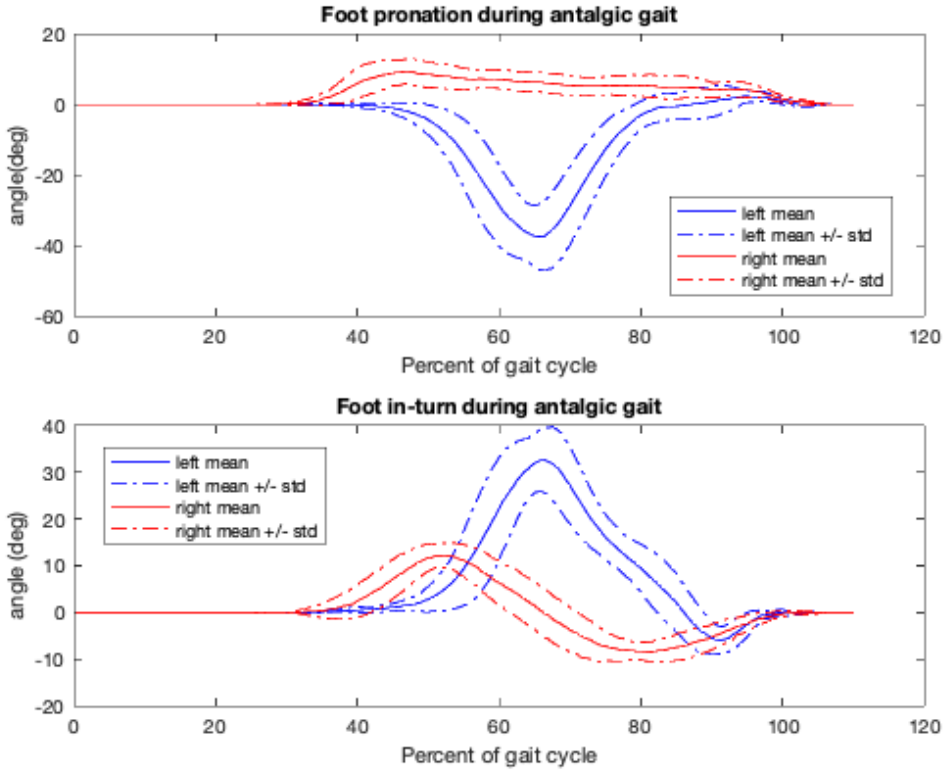

Figure 19. Foot pronation and in-turn for a sample of antalgic gait.

Figure 20 shows the x and z position of the sensor for a sample of antalgic gait. The first note corresponds with what was seen in the table of gait temporal parameters, that the left foot spends less time in swing phase, resulting in a steeper increase in x-position and a more compressed curve in z-position for the left foot. Despite this change, the step length remains similar for each foot. Although both are shorter than step lengths found in normal gait. One interesting change is the decrease in the first foot clearance and increase in the second foot clearance compared to normal gait.

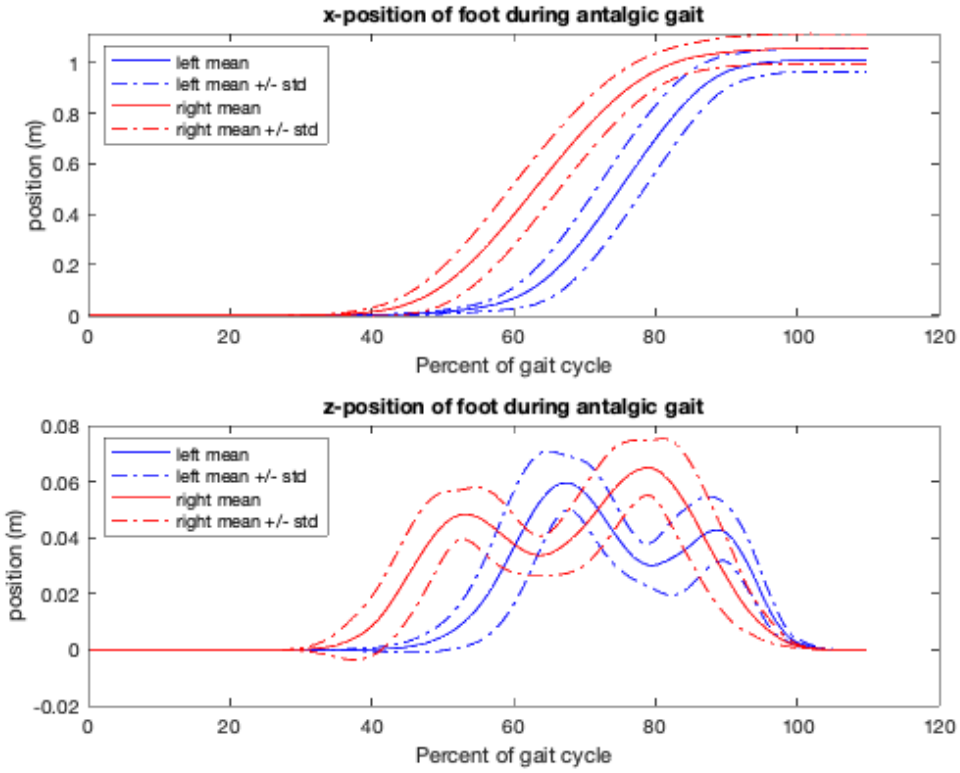

Figure 20. x and z position of foot for a sample of antalgic gait.

Figure 21 shows the x and z position trajectories of the feet during antalgic gait. Again, this figure shows similar information to what is available in the figure of x and z position above. Most importantly the decrease in the height of the first foot clearance and increase of the height of the second foot clearance for the right foot. It also shows that the minimum foot clearances are relatively similar between left and right.

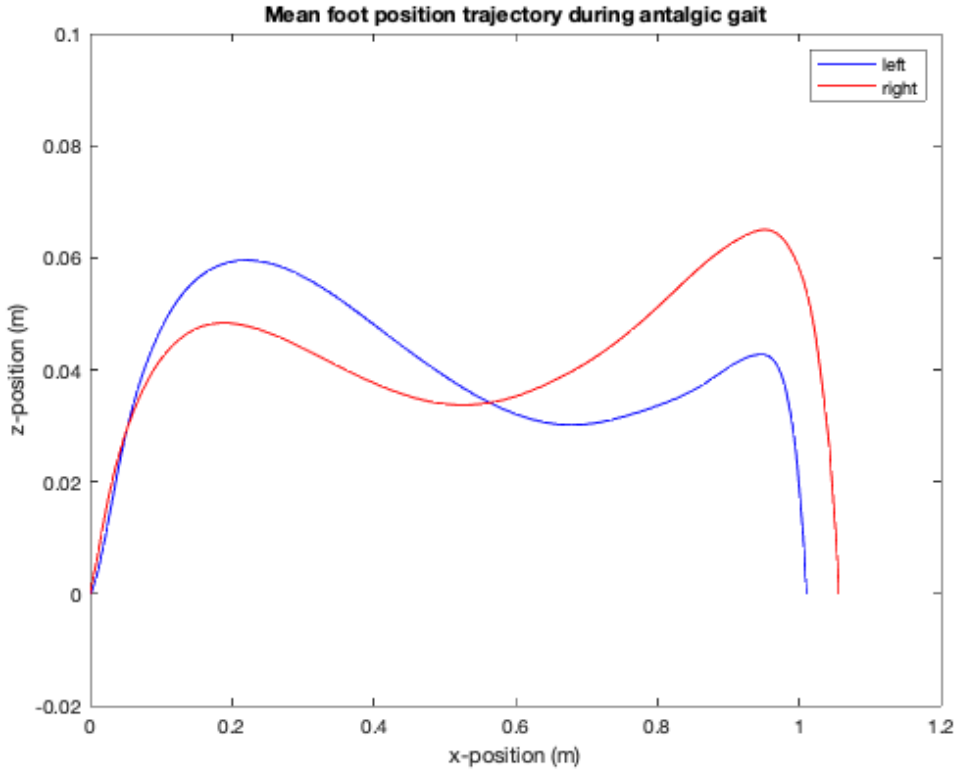

Figure 21. x and z position trajectory for a sample of antalgic gait.

Table 13 below shows the orientation and position parameters for the same sample of antalgic gait. Again, this table mostly shows what can already be inferred to the figures representing antalgic gait. The lack of pronation and in-turn in in the right foot is exhibited in the high value of minimum pronation and low value of maximum in-turn. The decrease in first foot clearance and increase in second foot clearance of the right foot compared to normal are also exhibited in the table. Finally, it shows that the step lengths of the right and left feet, although similar to one another are both shorter than the step lengths exhibited in normal gait.

Table 13. Table of orientation and position parameters for a sample of antalgic gait

	Left Mean	Right Mean	Symmetry
Max Pronation (deg)	4.591	11.717	0.392
Min Pronation (deg)	-44.524	-0.434	102.646
Max In-Turn (deg)	38.235	14.054	2.721
Min In-Turn (deg)	-8.188	-10.165	0.806
Foot Clearance 1 (m)	0.067	0.052	1.298
Foot Clearance 2 (m)	0.050	0.072	0.695
Min Foot Clearance (m)	0.024	0.026	0.911
Step Length (m)	1.010	1.056	0.956

The following figures and table represent limited mobility gait. This was collected with a rigid object holding the left knee joint in an extended position. Figure 22 shows the changes in pronation and in-turn. Recalling from the gait temporal parameters for limited mobility gait it is known that the right foot experiences a significantly shorter swing phase. It was postulated that this may be due to the participant feeling a sense of imbalance on the immobilized left leg during the right swing phase. This is supported by the significant increase in standard deviation of right foot pronation during swing phase which could be a result of the participant using the right foot to balance while in swing. Additionally, the right foot is found to experience a greater degree of pronation during swing phase. However, similar to in antalgic gait this could rather be due to greater supination during right stance phase, presumably to counterbalance the outward movement of the left leg in swing to provide clearance without the ability to flex the knee joint. This change in swing of the left foot is also represented by a muted supination and in-turn during swing, indicating that the foot is not rolling over the toes in the same way that it was during normal gait.

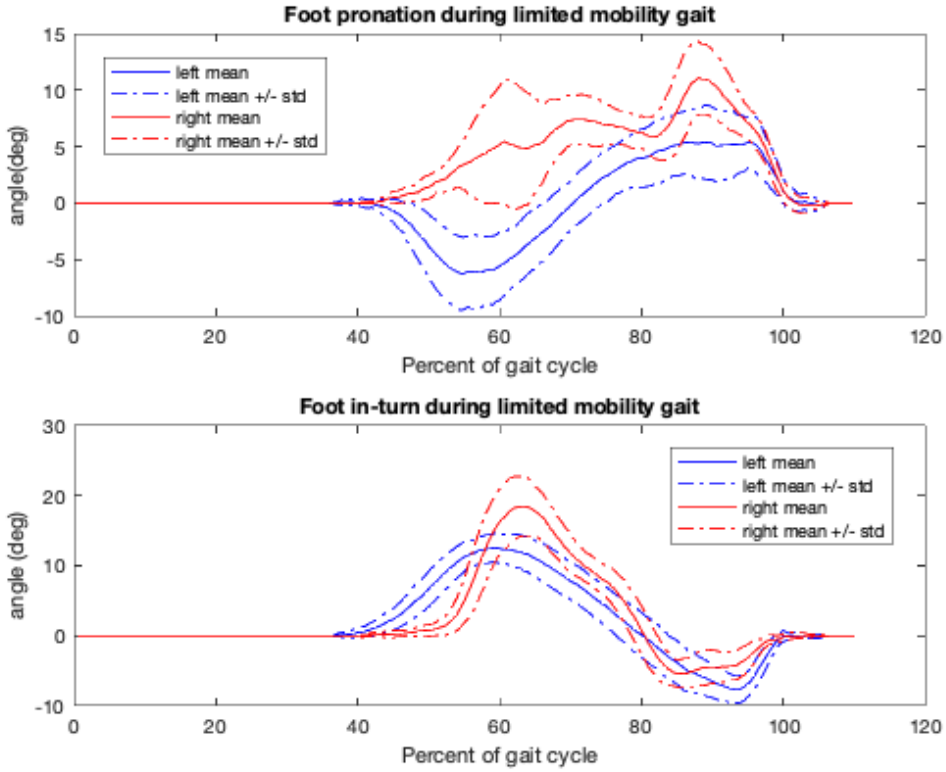

Figure 22. Foot pronation and in-turn for a sample of limited mobility gait.

Figure 23 shows the x and z position of the foot during limited mobility gait. This figure also shows the decrease in swing time seen in the GTP table. It manifests here as a much steeper curve in x-position and a more compressed shape in z-position for the right foot. Otherwise, the step lengths are similar to one another although, similar to antalgic gait, both are shorter than what was seen in normal gait. Another change is in the z-position of the left foot. For this sample of limited mobility gait, all foot clearance values are significantly lower that with normal gait showing the difficulty of providing foot clearance during the swing phase of the left foot, when flexion of the knee is not possible. Finally, it was noticed that the first foot clearance for the right foot was lower than was found in normal gait.

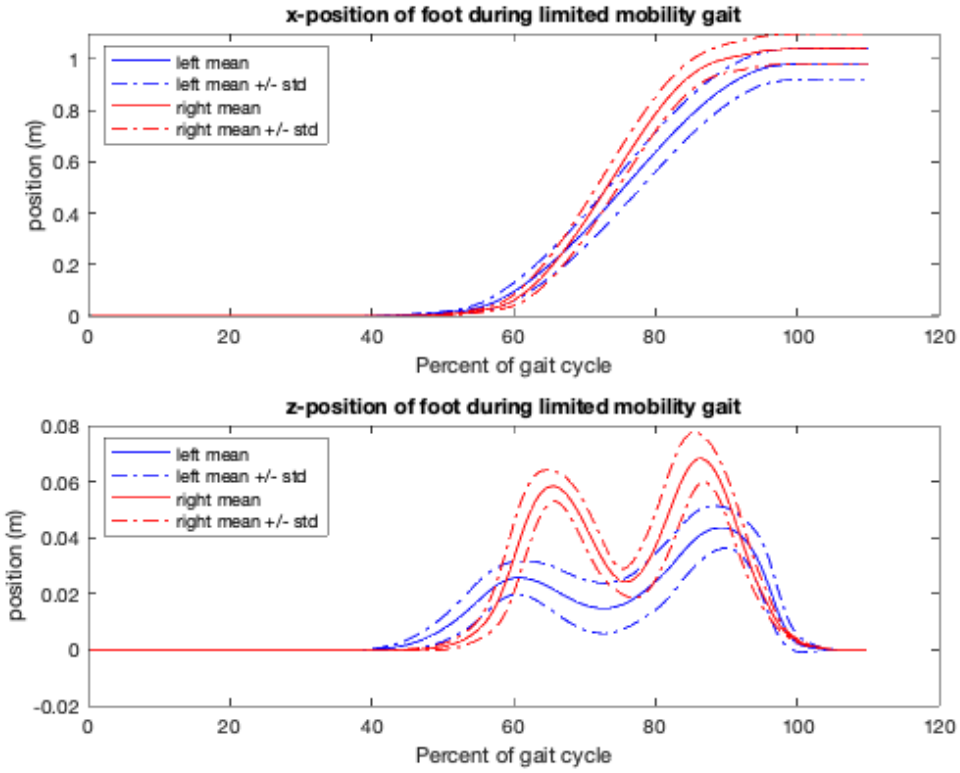

Figure 23. x and z position of foot for a sample of limited mobility gait.

Figure 24 shows the x and z position trajectory for a sample of limited mobility gait. Again, this figure shows information similar to the previous figure showing x and z position for limited mobility gait. It shows the low foot clearance of the left foot and the lower first foot clearance of the right foot. It is worth noting just how small this minimum foot clearance is, with only 1.4cm of clearance for the left foot in mid swing.

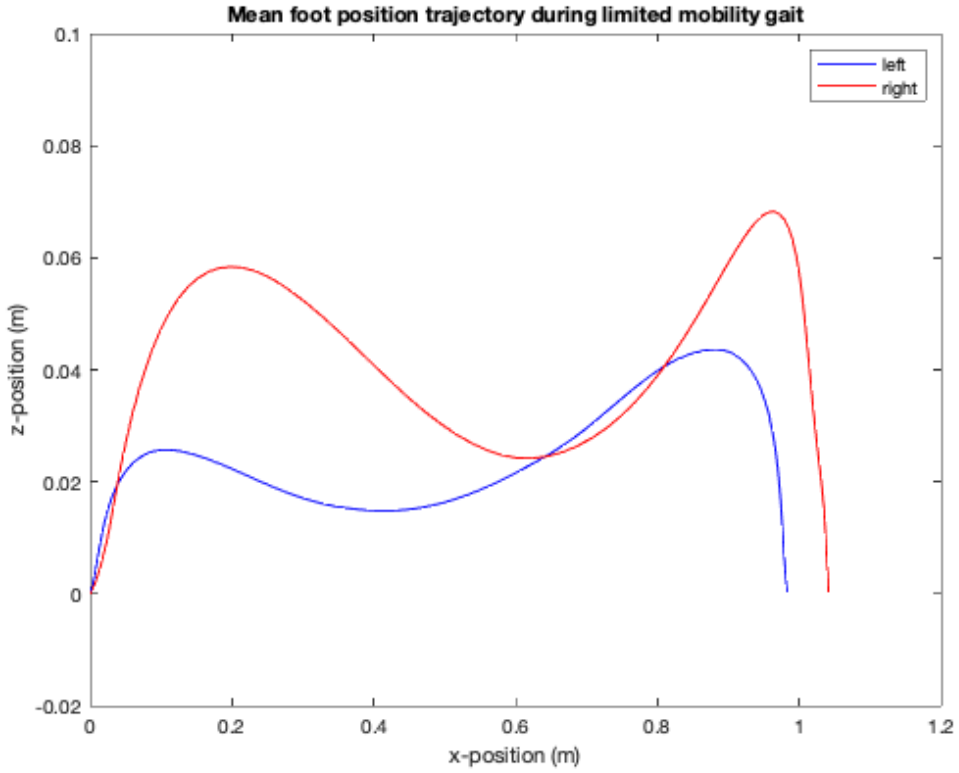

Figure 24. x and z position trajectory for a sample of limited mobility gait.

Table 14 below shows the orientation and position parameters for the same sample of limited mobility gait. This table basically quantifies what was visible in the figures. For example, it shows an increase in the minimum pronation angle compared to normal, indicating a lower degree of supination compared to the orientation during the flat foot phase. It also shows the decrease in the maximum in-turn of the left foot compared to normal. In terms of position, the table clearly shows the decrease in step length of both feet compared to normal as well as the decreases in foot clearance values for the left foot and the decrease in first foot clearance for the right foot.

Table 14. Table of orientation and position parameters for a sample of limited mobility gait

	Left Mean	Right Mean	Symmetry
Max Pronation (deg)	7.269	12.502	0.581
Min Pronation (deg)	-7.273	-1.399	5.199
Max In-Turn (deg)	13.747	19.662	0.699
Min In-Turn (deg)	-8.388	-6.944	1.208
Foot Clearance 1 (m)	0.027	0.060	0.453
Foot Clearance 2 (m)	0.045	0.070	0.648
Min Foot Clearance (m)	0.014	0.022	0.623
Step Length (m)	0.983	1.041	0.944

Together, these figures and tables demonstrate the observed differences in orientation and position for three different kinds of gait. The implications, impacts, and future improvements of these measurements will be discussed in the following chapter.

7. DISCUSSION

It was shown that packet loss was not found when collecting at 250Hz. At 333Hz a small number of packets were lost which were not consecutive. In the future, 333Hz could be considered viable if the project required higher sampling rates, while willing to sacrifice a small percentage (~0.3%) of packets. At 500Hz, packet loss was significant, and the resultant observed sampling rates were less consistent and lower on average than when sampling at 333Hz for this reason there is no foreseeable reason why anyone would use this sensor unit to sample at 500Hz.

The labelling algorithm was found to be effective at labeling each sensor for all of the trials collected between two participants and three different simulated gait conditions. This suggests that the algorithm would be robust to different styles of gait. However, it is possible that unforeseen gait patterns may confuse the algorithm. One way that this could occur would be if a participant has a different foot shape. This is because the differentiation between the right and left feet is made by the y-axis of the foot sloping slightly up or down, on the right or left feet, respectively. Therefore, if the feet have a different shape then it could cause the sensors to improperly differentiate between right and left. If this is the case, then it would be prudent to implement further methods for distinguishing between right and left in the future. Another future action that could be taken would be to apply an artificial neural network that labels the signal based on many labeled samples. However, this method and other potential machine learning methods were considered to be out of the scope of this project.

The gait event detection and segmentation algorithm was found to be effective in detecting gait events in normal gait and two different kinds of abnormal gait resulting from a painful sensation in the right foot or the immobilization of the left knee joint. These results were verified through inspection and through comparison with accelerometer data to identify gait events. The small differences that were found in the location of IFC events could be explained by inertial of the sensor and imperfect connection to the body segment causing the sensor to still be moving slightly, even after the body segment has reached a resting position. Accurate detection of gait events is critical, because it determines the accuracy of the gait temporal parameters. In the future, it would be worthwhile to compare the gait events produced by the algorithms to those produced by a gold standard system such as a force plate or foot switches to ensure accuracy.

Additionally, it is important to not falsely detect gait segments which are really just artefacts of the IMU signal. The developed algorithm deals with these quite simply, by determining if all gait events are occurring in the correct order and in a realistic time frame, removing the segments that do not meet these criteria. Unfortunately, this has the consequence of removing some real events which do not occur as expected. This could limit the alter the algorithms ability to work with severely altered gait in the future. However, this was considered to be a worthwhile trade-off, because the IMU allows for the collection of such large amounts of data at rather low cost. This means that even if a significant percentage of gait segments are erroneously removed there will still be a wealth of data on which to preform analysis. The true consequence is that for significantly altered gait it could introduce bias to only show the more normal gait. This balance of specificity should continually be reconsidered, particularly when the system is applied to significantly altered gait.

Accurate detection of gait events and segments is essential for the accuracy of all of the data which is extracted from those segments. The first of which are the gait

temporal parameters (GTP). Because GTP are just temporal comparisons between gait event, they only require two things. Accurate time data, which is provided by the real time clock RTC and accurate gait event detection. The GTP collected for this project seemed accurate and were repeatable for the same individual, demonstrating a high level of relative validity. It was noticeable how GTP change with different styles of gait showing the ability of these metrics to identify abnormal gait. However, further validation could be done by comparing to a gold standard system of force plates or foot switches.

The most ambitious measurements in this project are the trajectories of orientation and position as well as their associated parameters. These measurements are considered ambitious, because they are difficult to deliver accurately using IMU sensors due to external influences on the IMU as well as the characteristic integration drift. As mentioned in chapter 5, many assumptions were made to better manage this integration drift. The most notable assumptions being that the foot returns to a normal flat foot position during the stance phase of each segment. It was seen in section 6.5 that this may not always be the case for patterns of abnormal gait. In particular, the sample of antalgic gait which showed the foot becoming more supinated during swing phase may have been hiding the real effect which was that the foot was in a more supinated position during the stance phase. This is one of the ways in which the assumptions made could mask what is really happening. Despite this negative effect, the other assumptions seem to have few noticeable effects. For example, the assumption of zero velocity during each flat foot phase is likely always true unless the foot is slipping, or the ground is somehow moving. In fact, this assumption even helped to remove the effect of the sensors moving after the foot impacts the ground. Knowing that velocity should be zero after IFC allows for the elimination of the transient acceleration signal caused by the oscillation of the sensor. Finally, the assumption that the foot always returns to a vertical height of zero was essential and did not show any noticeable side-effects. It is considered essential, because of the small scale of the foot clearance measurements, even a change of a few millimeters could be significant.

Measurements of orientation and position were used to construct gait parameters including foot clearances step lengths and maximum angles of pronation and supination compared to the flat foot phase. These parameters were selected to demonstrate how orientation and position information can be summarized very briefly by only a few different parameters. These parameters enable diagnosis when fed into machine learning algorithms to diagnose disease or act as a quick reference for physicians when administering rehabilitation. They are essential the final output of all of the algorithms included in this thesis and as such, their accuracy is critical.

For the clearance measurements and other orientation and position parameters, accuracy is important. Because there was no ground truth for comparison in this project, validation was left to a measurement of how similar the results were between different segments and between different trials. It was found that for most trials the behavior was similar, indicating strong repeatability, however there were still some trials which produced abnormal and potentially erroneous results. A particularly strong example of this was found when measuring the z-position over time. It was found that in rare cases the z-position at minimum clearance would be below zero. Although trial means constructed from the segments were still normal, these outliers provide reason for concern. They also show one of the fundamental issues with position tracking using IMU, that drift is not entirely avoidable. Although drift can be compensated for through making assumptions, there is still time for bias to accumulate before it can be

corrected. This raises some mild concerns about the validity of IMU position tracking which should be further studied in the future. A good place to start with this would be to use a gold standard method such as motion capture and compare the result to the position trajectory created by the IMU. Motion capture could also be used to test orientation measurements by attaching frame markers to the feet.

In the future, more attention should be paid to absolute validation. This includes comparison to the gold standard methods mentioned above. Once these methods are validated, they can be used safely and reliably to collect gait data outside of the laboratory. Once this occurs, the amount of data being collected will increase dramatically. With large amounts of data, from many sources, and many different styles of gait a new opportunity arises to replace the hard coded algorithms in this work with machine learning equivalents. Machine learning algorithms could be applied to pre-process gait data based on large amounts of previously labelled data. This could identify patterns that are not recognizable by human observers. It could also better quantify existing patterns. Machine learning could benefit the labelling algorithm by identifying more features that distinguish between foot and shank sensors, of which there are many. This could lead to a more robust labelling algorithm, particularly for abnormal gait patterns. Machine learning could also be beneficial in the identification of gait events by incorporating data from both the accelerometer and gyroscope to identify gait event location. It could also be used to discard segments which contain signal artefacts rather than actual gait events. As the amount of labelled gait data increases, these algorithms could continually improve providing a more future-proof solution than the hard-coded algorithms presented. However, the algorithms in this project do provide a fundamental stepping-stone to this future. By creating and labelling data, the outputs of the current algorithms could label the datasets which enable the gait processing algorithms of the future.

8. CONCLUSION

The study of gait is being improved through quantification. IMU provides a method of gait quantification which enables gait data to be collected outside of the laboratory and at a relatively low cost compared to other gold standard equipment for gait analysis. This enables the collection and processing of vast amounts of gait data which does not rely on professional observation or processing.

This thesis provides a framework for the automated analysis of gait data which is essential for effectively processing large quantities of gait data. The algorithms were found to be effective in labelling sensors, detecting gait events, segmenting gait data according to the four-phase gait model, and producing trajectory and parameters measurements for the orientation and position of the foot sensors. Although testing was successful for two participants and for three different styles of gait, the scope of the testing population is still very narrow and should be expanded in future work. Abnormal gait simulated in this work provided an opportunity to see how the system would react to non-neural gait impairments. Future work should include neural impairments to gait, such as dual task walking or other conditions with a known impact of the patterns of gait to see the changes that these neural impairments evoke. In both cases, comparison should be made to a gold standard measurement system to ensure accuracy.

9. REFERENCES

[1] R. Baker, *Measuring Walking: A Handbook of Clinical Gait Analysis*. London: Mac Keith Press, 2013.

[2] B. E. Maki, P. J. Holliday, and A. K. Topper, "Fear of Falling and Postural Performance in the Elderly," *Journals of Gerontechnology*, vol. 46, no. 4, pp. M123–M131, 1991.

[3] A. H. Snijders, B. P. Van De Warrenburg, N. Giladi, and B. R. Bloem, "Neurological gait disorders in elderly people: clinical approach and classifi cation," 2007.

[4] D. K. White *et al.*, "Trajectories of Gait Speed Predict Mortality in Well-Functioning Older Adults: The Health, Aging and Body Composition Study," *Journals Gerontol. Ser. A Biol. Sci. Med. Sci.*, vol. 68, no. 4, pp. 456–464, Apr. 2013, doi: 10.1093/gerona/gls197.

[5] E. Sejdić, Y. Fu, A. Pak, J. A. Fairley, and T. Chau, "The Effects of Rhythmic Sensory Cues on the Temporal Dynamics of Human Gait," *PLoS One*, vol. 7, no. 8, p. e43104, Aug. 2012, doi: 10.1371/journal.pone.0043104.

[6] A. Mannini, D. Trojaniello, A. Cereatti, and A. M. Sabatini, "A machine learning framework for gait classification using inertial sensors: Application to elderly, post-stroke and huntington's disease patients," *Sensors (Switzerland)*, vol. 16, no. 1, Jan. 2016, doi: 10.3390/s16010134.

[7] N. B. Alexander, "Gait Disorders in Older Adults," 1996.

[8] E. P. Washabaugh, T. Kalyanaraman, P. G. Adamczyk, E. S. Claflin, and C. Krishnan, "Validity and repeatability of inertial measurement units for measuring gait parameters," 2017, doi: 10.1016/j.gaitpost.2017.04.013.

[9] T. B. Rodrigues, D. P. Salgado, C. Catháin, N. O'Connor, and N. Murray, "Human gait assessment using a 3D marker-less multimodal motion capture system," *Multimed. Tools Appl.*, vol. 79, no. 3–4, pp. 2629–2651, Jan. 2020, doi: 10.1007/s11042-019-08275-9.

[10] M. Kyrarini, X. Wang, and A. Graser, "Comparison of vision-based and sensor-based systems for joint angle gait analysis," in *2015 IEEE International Symposium on Medical Measurements and Applications (MeMeA) Proceedings*, 2015, pp. 375–379, doi: 10.1109/MeMeA.2015.7145231.

[11] A. Pfister, A. M. West, S. Bronner, and J. A. Noah, "Comparative abilities of Microsoft Kinect and Vicon 3D motion capture for gait analysis," *J. Med. Eng. Technol.*, vol. 38, no. 5, pp. 274–280, 2014, doi: 10.3109/03091902.2014.909540.

[12] A. M. Sabatini, C. Martelloni, S. Scapellato, and F. Cavallo, "Assessment of walking features from foot inertial sensing," *IEEE Trans. Biomed. Eng.*, vol. 52, no. 3, pp. 486–494, Mar. 2005, doi: 10.1109/TBME.2004.840727.

[13] M. I. Mohamed Refai, B.-J. F. van Beijnum, J. H. Buurke, and P. H. Veltink, "Gait and Dynamic Balance Sensing Using Wearable Foot Sensors," *IEEE Trans. Neural Syst. Rehabil. Eng.*, vol. 27, no. 2, pp. 218–227, Feb. 2019, doi: 10.1109/TNSRE.2018.2885309.

[14] U. Qureshi and F. Golnaraghi, "An Algorithm for the In-Field Calibration of a MEMS IMU," *IEEE Sens. J.*, vol. 17, no. 22, pp. 7479–7486, Nov. 2017, doi: 10.1109/JSEN.2017.2751572.

[15] R. Gao and L. Zhang, "Micromachined microsensors for manufacturing," *IEEE Instrum. Meas. Mag.*, vol. 7, no. 2, pp. 20–26, Jun. 2004, doi:

10.1109/MIM.2004.1304562.
[16] N. Yazdi, F. Ayazi, and K. Najafi, “Micromachined inertial sensors,” *Proc. IEEE*, vol. 86, no. 8, pp. 1640–1658, 1998, doi: 10.1109/5.704269.
[17] V. Beroulle, Y. Bertrand, L. Latorre, and P. Nouet, “Monolithic piezoresistive CMOS magnetic field sensors,” *Sensors Actuators, A Phys.*, vol. 103, no. 1–2, pp. 23–32, Jan. 2003, doi: 10.1016/S0924-4247(02)00317-5.
[18] J. Taborri, E. Palermo, S. Rossi, and P. Cappa, “Gait partitioning methods: A systematic review,” *Sensors (Switzerland)*, vol. 16, no. 1, Jan. 2016, doi: 10.3390/s16010066.
[19] J. M. Jasiewicz *et al.*, “Gait event detection using linear accelerometers or angular velocity transducers in able-bodied and spinal-cord injured individuals,” *Gait Posture*, vol. 24, no. 4, pp. 502–509, 2006, doi: 10.1016/j.gaitpost.2005.12.017.
[20] G. Pacini Panebianco, M. C. Bisi, R. Stagni, and S. Fantozzi, “Analysis of the performance of 17 algorithms from a systematic review: Influence of sensor position, analysed variable and computational approach in gait timing estimation from IMU measurements,” *Gait Posture*, vol. 66, pp. 76–82, Oct. 2018, doi: 10.1016/j.gaitpost.2018.08.025.
[21] A. M. Sabatini, “Estimating Three-Dimensional Orientation of Human Body Parts by Inertial/Magnetic Sensing,” *Sensors*, vol. 11, no. 2, pp. 1489–1525, Jan. 2011, doi: 10.3390/s110201489.
[22] N. Yadav and C. Bleakley, “Accurate orientation estimation using AHRS under conditions of magnetic distortion,” *Sensors (Switzerland)*, vol. 14, no. 11, pp. 20008–20024, Oct. 2014, doi: 10.3390/s141120008.
[23] T. Seel, J. Raisch, T. Schauer, T. Seel, J. Raisch, and T. Schauer, “IMU-Based Joint Angle Measurement for Gait Analysis,” *Sensors*, vol. 14, no. 4, pp. 6891–6909, Apr. 2014, doi: 10.3390/s140406891.
[24] T. Seel, D. Graurock, and T. Schauer, “Realtime assessment of foot orientation by Accelerometers and Gyroscopes,” *Curr. Dir. Biomed. Eng.*, vol. 1, no. 1, pp. 446–469, Sep. 2015, doi: 10.1515/cdbme-2015-0112.
[25] Q. Li, M. Young, V. Naing, and J. M. Donelan, “Walking speed estimation using a shank-mounted inertial measurement unit,” *J. Biomech.*, vol. 43, no. 8, pp. 1640–1643, 2010, doi: 10.1016/j.jbiomech.2010.01.031.
[26] N. Kitagawa and N. Ogihara, “Estimation of foot trajectory during human walking by a wearable inertial measurement unit mounted to the foot,” *Gait Posture*, vol. 45, pp. 110–114, Mar. 2016, doi: 10.1016/j.gaitpost.2016.01.014.
[27] D. Roetenberg, P. J. Slycke, and P. H. Veltink, “Ambulatory position and orientation tracking fusing magnetic and inertial sensing,” *IEEE Trans. Biomed. Eng.*, vol. 54, no. 5, pp. 883–890, May 2007, doi: 10.1109/TBME.2006.889184.
[28] M. Grimmer, K. Schmidt, J. E. Duarte, L. Neuner, G. Koginov, and R. Riener, “Stance and swing detection based on the angular velocity of lower limb segments during walking,” *Front. Neurorobot.*, vol. 13, 2019, doi: 10.3389/fnbot.2019.00057.
[29] L. Ricci, F. Taffoni, and D. Formica, “On the Orientation Error of IMU: Investigating Static and Dynamic Accuracy Targeting Human Motion,” *PLoS One*, vol. 11, no. 9, p. e0161940, Sep. 2016, doi: 10.1371/journal.pone.0161940.
[30] J. Bae *et al.*, “A lightweight and efficient portable soft exosuit for paretic ankle assistance in walking after stroke,” in *Proceedings - IEEE International*

Conference on Robotics and Automation, 2018, pp. 2820–2827, doi: 10.1109/ICRA.2018.8461046.

[31] J. Barth *et al.*, "Biometric and mobile gait analysis for early diagnosis and therapy monitoring in Parkinson's disease," in *Proceedings of the Annual International Conference of the IEEE Engineering in Medicine and Biology Society, EMBS*, 2011, pp. 868–871, doi: 10.1109/IEMBS.2011.6090226.

[32] F. Cuzzolin *et al.*, "Metric learning for Parkinsonian identification from IMU gait measurements," 2017, doi: 10.1016/j.gaitpost.2017.02.012.

[33] D. Luksys *et al.*, "Neurological diseases differentiation analysis using inertial measurement units," in *2016 IEEE 4th Workshop on Advances in Information, Electronic and Electrical Engineering, AIEEE 2016 - Proceedings*, 2017, doi: 10.1109/AIEEE.2016.7821814.

[34] Hillcrest Labs, "FSM - 9 Data Sheet," 2013.

[35] X. Wang, M. Kyrarini, D. Ristic-Durrant, M. Spranger, and A. Graser, "Monitoring of gait performance using dynamic time warping on IMU-sensor data," in *2016 IEEE International Symposium on Medical Measurements and Applications (MeMeA)*, 2016, pp. 1–6, doi: 10.1109/MeMeA.2016.7533745.

[36] Hillcrest Labs, "HCOMM Reference Manual," 2013.